

SPECTROSCOPIC ANALYSIS OF DA WHITE DWARFS: STARK BROADENING OF HYDROGEN LINES INCLUDING NON-IDEAL EFFECTS

P.-E. Tremblay and P. Bergeron

*Département de Physique, Université de Montréal, C.P. 6128, Succ. Centre-Ville,
Montréal, Québec H3C 3J7, Canada.*

tremblay@astro.umontreal.ca, bergeron@astro.umontreal.ca

ABSTRACT

We present improved calculations for the Stark broadening of hydrogen lines in dense plasmas typical of white dwarf atmospheres. Our new model is based on the unified theory of Stark broadening from Vidal, Cooper, & Smith. For the first time, we account for the non-ideal effects in a consistent way directly inside the line profile calculations. The Hummer & Mihalas theory is used to describe the non-ideal effects due to perturbations on the absorber from protons and electrons. We use a truncation of the electric microfield distribution in the quasi-static proton broadening to take into account the fact that high electric microfields dissociate the upper state of a transition. This approach represents a significant improvement over previous calculations that relied on the use of an ad hoc parameter to mimic these non-ideal effects. We obtain the first model spectra with line profiles that are consistent with the equation of state. We revisit the properties of DA stars in the range $40,000 \text{ K} > T_{\text{eff}} > 13,000 \text{ K}$ by analyzing the optical spectra with our improved models. The updated atmospheric parameters are shown to differ substantially from those published in previous studies, with a mean mass shifted by $+0.034 M_{\odot}$. We also show that these revised atmospheric parameters yield absolute visual magnitudes that remain in excellent agreement with trigonometric parallax measurements.

Subject headings: white dwarfs — stars: atmospheres — line: profiles

1. INTRODUCTION

The most successful technique used to determine the effective temperatures and surface gravities of hydrogen-line DA white dwarfs is to compare the observed and predicted hydrogen line profiles. This so-called spectroscopic technique was first applied to a large sample of

DA stars by Bergeron et al. (1992, hereafter BSL92) in the case of the hydrogen Balmer lines. In recent years, the method has also been applied to the study of the Lyman line profiles in the ultraviolet (Barstow et al. 2003; Vennes et al. 2005). The success of this approach resides in the fact that the theoretical line profiles are very sensitive to variations of the atmospheric parameters (Wegner & Schulz 1981). This is illustrated in Figure 1 where the theoretical profiles of five Balmer lines are displayed for various values of T_{eff} and $\log g$. In comparison with the other fitting methods used before (see BSL92 for an extensive review), the spectroscopic method has the lowest intrinsic uncertainties, which allows for a more precise comparison, at least in a relative sense, of the atmospheric parameters between different DA stars. For instance, BSL92 used the spectroscopic method to determine the shape of the DA mass distribution (see also Liebert et al. 2005; Kepler et al. 2007), while Bergeron et al. (1995b) applied the same method to define the location of the ZZ Ceti instability strip in a $\log g - T_{\text{eff}}$ diagram (see also Gianninas et al. 2006). Since about 80% of the white dwarf population is of the DA type, the spectroscopic technique coupled with high signal-to-noise spectroscopic observations of the Balmer lines for large samples of DA stars (Gianninas et al. 2005; Eisenstein et al. 2006) can reveal important details about the luminosity function and the evolution and the formation rate of DA white dwarfs (Liebert et al. 2005).

Even though the *relative* accuracy of the spectroscopic method is mostly limited by the quality of the observations (signal-to-noise ratio, flux calibration, etc.), the *absolute* values of the atmospheric parameters depend highly on the level of sophistication of the physics included in the calculations of model atmospheres with hydrogen-rich compositions. One starting point would be the efficient code of Wesemael et al. (1980) that allowed for the computation of radiative LTE atmospheres for hot DA white dwarfs. Similar codes have also been developed by D. Koester and described in Finley et al. (1997). Since then, the most important advance has certainly been the inclusion of NLTE effects — in the code of Hubeny & Lanz (1995) among others — which allowed the study of hot DA stars ($T_{\text{eff}} > 40,000$ K). In terms of cooler white dwarfs, the code developed by Bergeron et al. (1991) made great advances and has been a reference ever since. It includes convective energy transport and the non-ideal equation of state of Hummer & Mihalas (1988, hereafter HM88) to describe the atomic populations. Otherwise, it is mostly in the atomic physics, with new or improved opacities and partition functions, that advances have been made.

The dominant features observed in DA spectra are the hydrogen lines. It is thus important to have a good understanding of the atomic transitions to exploit the power of the spectroscopic technique to its fullest. The main source of line broadening in most DA stars ($T_{\text{eff}} > 10,000$ K) is due to charged particle interactions, also called Stark broadening. The theory that has been the most successful to describe these line profiles is the unified theory of Stark broadening from Vidal, Cooper, & Smith (1970, hereafter VCS; see also

Smith et al. 1969; Vidal et al. 1971, 1973). This theory was used right from the beginning in the analysis of large samples of DA white dwarfs (BSL92) and it is the basis of most of the widely accepted results on the global properties of these stars. Even though the theoretical framework of the unified theory has been known since the original work of VCS, it is not until the calculations of Lemke (1997) that a complete grid of hydrogen line profiles from the unified theory became available, covering the full range of possible transitions, temperatures, and electronic densities encountered in DA white dwarf atmospheres. Before that, line profiles from the unified theory were either extrapolated to high densities (T. Schönig and K. Butler, private communication), or more drastically, less accurate broadening theories (Underhill & Waddell 1959; Edmonds et al. 1967) were used for the highest lines of the Balmer series (H ϵ and above). At T_{eff} below $\sim 10,000$ K for the Balmer lines and below 30,000 K for the Lyman lines, other types of line broadening, mostly due to neutral particles, must be included in the model atmospheres. The modeling of the quasi-molecular line opacity (Allard et al. 2004) has been one of the most significant advance in this domain.

Despite the development of these theoretical tools, the study of DA stars has suffered from several complications. For instance, in their preliminary analysis of 129 DA white dwarfs, BSL92 discovered a lack of internal consistency between the spectroscopic solutions obtained when an increasing number of Balmer lines were included in the fitting procedure. This is illustrated at the top of Figure 2 for a typical DA white dwarf where we can see that the solution drifts in the T_{eff} vs $\log g$ diagram as more lines are included in the fit. This correlation indicates that the physics included in the model calculations needed significant improvement. Bergeron (1993) traced back the problem to the neglect of non-ideal effects inside the Stark broadening calculations. Indeed, Seaton (1990) had argued that non-ideal effects, such as those taken into account in the HM88 equation of state, have also to be included directly in the line profile calculations to get a coherent physical framework. However, it was not possible at the time of the analysis of BSL92 to rework the line broadening calculations. Instead, the authors chose to include an ad hoc parameter inside the model atmosphere code to *mimic* the non-ideal effects in the line profiles (Bergeron 1993). By taking twice the value of the critical electric microfield (β_{crit} , see § 2.3) from the HM88 theory, it was found that the internal consistency improved substantially, as can be seen in the middle panel of Figure 2. *It should be stressed, however, that this does not imply that HM88 underestimated the value of the critical field.* This is just a quick and dirty way to simulate the non-ideal effects by reducing the line wing opacity, in particular where the line wings overlap (see Bergeron 1993 for further details). This ad hoc parameter has been used ever since in all model spectra of white dwarf stars (BSL92; Hubeny & Lanz 1995; Finley et al. 1997; Kawka & Vennes 2006).

In this paper, we solve the problem discussed above in a more elegant way, by computing

improved Stark broadening profiles based of the unified theory of VCS, but by including non-ideal effects directly in the line profile calculations following an approach similar to that originally proposed by Seaton (1990). The non-ideal effects due to the proton and electron perturbations are taken into account using the HM88 theory. We begin in § 2 by discussing the two successful theories at the heart of our calculations, namely the VCS unified theory of Stark broadening and the HM88 non-ideal equation of state. In § 3, we describe how these two formalisms are combined for the first time to compute Stark broadening profiles that take into account non-ideal effects. We then evaluate in § 4 the implications of our improved line profiles on the spectroscopic analysis of DA stars. Our conclusions follow in § 5.

2. LINE BROADENING THEORY

The basis of model atmospheres for DA white dwarfs resides in the equation of state and opacity calculations of the hydrogen gas. One of the most successful equations of state used to compute the populations of the different accessible states (bound states of hydrogen, H^- , molecular H_2 , H_2^+ and H_3^+ , as well as proton and electron populations) is the HM88 non-ideal equation of state described in more detail in section § 2.2. With these populations in hand for all states of the gas, we can proceed to calculate the gas opacity, which is generally split into true absorption and scattering processes. In particular, the bound-bound opacity (or line opacity) between one initial state i and one final state j is written as

$$\kappa_{ij}(\nu) d\nu = N_i \frac{\pi e^2}{m_e c} f_{ij} \phi(\nu) d\nu , \quad (1)$$

where N_i is the population of the initial state and f_{ij} is the oscillator strength of the transition. These two factors define the amplitude of the transition while $\phi(\nu)$ is the spectral broadening profile normalized to unity. In this paper, we are mostly interested in the broadening profile for the hydrogen lines. This opacity is the key ingredient of the spectroscopic method that relies on a detailed comparison of observed and predicted line profiles.

Generally speaking, the line profile is a convolution of different broadening mechanisms. The first source of broadening is due to the interaction between the absorber and the charged particles in the plasma. This process is referred to as Stark broadening and is discussed in more detail in section § 2.1. Stark broadening represents the dominant source of broadening for most transitions in DA white dwarfs. Accounting only for this source of broadening, the line profile can be expressed (Underhill & Waddell 1959; Edmonds et al. 1967) as

$$\phi(\nu) d\nu = \frac{\lambda^2}{cF_0} S^*(\alpha) d\nu , \quad (2)$$

where $\alpha = \Delta\lambda/F_0$ with $\Delta\lambda$ measured from the center of the line. F_0 is defined as the electric field at the mean distance between the plasma ions

$$F_0 = Z_p e (4\pi N_p / 3)^{2/3} = 1.25 \times 10^{-9} Z_p N_e^{2/3} , \quad (3)$$

where Z_p and N_p are the charge and density of perturbers, respectively. The profile $S^*(\alpha)$ is a convolution of a pure Stark profile $S(\alpha)$ and a Voigt function $H(a, v)$ that takes into account thermal and natural broadening

$$S^*(\alpha) = \int_{-\infty}^{\infty} S\left(\alpha + \frac{\lambda_0 v}{F_0 c}\right) \frac{H(a, v)}{\sqrt{\pi}} dv , \quad (4)$$

where $a = \Gamma/4\pi\Delta\nu_D$, with Γ representing the natural broadening half-width and $\Delta\nu_D$ the Doppler width. The second type of broadening important in DA white dwarfs is the interaction of the absorber with neutral hydrogen. It is especially important at low effective temperatures for transitions involving an upper level with a low principal quantum number. In the case of Balmer lines, we must include resonance broadening (Ali & Griem 1965, 1966) and nonresonant broadening (Hammond et al. 1991) in cool white dwarfs with $T_{\text{eff}} < 10,000$ K. Since this source of broadening has a Lorentzian profile, the broadening parameter can be added directly to that of the natural broadening. For the lower Lyman lines ($L\alpha$, $L\beta$, and $L\gamma$), close range collisions of the absorber with hydrogen atoms and protons cause the appearance of important satellites in the wings of the lines that are visible up to $T_{\text{eff}} \sim 30,000$ K (Allard & Kielkopf 1982; Allard et al. 2004). This opacity also affects the thermodynamic structure of the atmosphere. Furthermore, at very low effective temperatures, H-H₂ collisions become the main source of broadening for $L\alpha$ (Kowalski & Saumon 2006).

2.1. Stark Broadening

The Stark effect is defined as the shifting — or splitting — of spectral lines under the action of an electric field. In the following section, we assume that we have in the atmospheric plasma a local electric microfield due to protons that is constant with time. This static approximation is well justified since the characteristic time for the fluctuation of the local microfield due to a change in the proton distribution is much larger than the characteristic time of absorption and emission processes that we are studying (Stehlé & Jacquemot

1993). We also assume that the microfield is constant in space, a good approximation if the perturbers are far from the area occupied by the bound electron orbits. The regime where this approximation fails is discussed further in § 2.3. The electric microfield, assumed to be along the z -axis, interacts with the dipolar moment of the atom and leads to a perturbation in the Hamiltonian of the form

$$H_s = e\vec{R} \cdot \vec{F} = eFz . \quad (5)$$

It is common to write the amplitude of the microfield in terms of the unitless parameter β such that

$$\beta = \frac{F}{F_0} , \quad (6)$$

where F_0 is the characteristic field defined by equation (3). The amplitude of the microfield can be expressed using a probability distribution $P(\beta)$. One such distribution that can be computed analytically is the Holtsmark distribution, which takes into account the interactions (vectorial sum) between the different perturbers. We use here the more physical distribution of Hooper (1968) that takes into account the Debye screening effect, and which corresponds also to the formulation included in the work of VCS. HM88 originally used the Holtsmark distribution, but for consistency we use the approach of Nayfonov et al. (1999) for the HM88 equation of state by replacing the Holtsmark distribution with the Hooper distribution. We note that this improved version of the HM88 equation of state is already included in our model atmosphere code, although it has never been properly documented.

We note that the perturbation H_s does not commute with the angular momentum \vec{L}^2 since it has a privileged direction in space. The effect of breaking this symmetry is to lift the degeneracy in energy of the hydrogen atomic levels. There are no exact solutions to this problem and we generally use quantum mechanical perturbation theory to determine corrections to the energy and wave functions. The first order corrections to the energy are linear in relation to the electric microfield that is applied, and represent the basis of the linear Stark effect. The linear corrections are found by diagonalizing the perturbation operator in the degenerate subspaces. For a hydrogen atom, we can write this expression analytically. First of all, knowing that the operator z conserves the azimuthal quantum number m , we can diagonalize the matrix $\langle \Psi_k | H_s | \Psi_l \rangle$ (Condon & Shortley 1935) by making use of the quantum numbers (n, m, q) , where $q = q_1 - q_2$ with $q_1 + q_2 = n - |m| - 1$, and n is the principal quantum number. The shifts in energy are then given by

$$\Delta E_{n,m,q}^1 = \frac{3ea_0F}{2}nq . \quad (7)$$

When the electric microfield becomes very high, or equivalently, when the Stark splitting is important enough that the Stark components of two levels with a different principal quantum number are crossing, the linear approximation is no longer valid. The second order corrections to the energy become quadratic in relation to the microfield, and we find

$$\Delta E_{n,m,q}^2 = e^2 F^2 \sum_{n' \neq n} \frac{|\langle \Psi_{n',m',q'} | z | \Psi_{n,m,q} \rangle|^2}{E_{n,m,q}^0 - E_{n',m',q'}^0}. \quad (8)$$

The problem with this perturbation approach to the Stark effect is that the wave functions, using any order of the perturbation theory, are not necessarily normalizable (Friedrich 2006). This is because the perturbing potential goes to $-\infty$ when z goes to $-\infty$. In other words, states that were bound without a microfield are now only metastable states, and there is a finite probability that the atom will be ionized when the microfield has a sufficiently high amplitude. Classically, the sum of the electric potentials of the absorber and the nearby protons only allows bound states in the local potential minima up to a certain energy, called the saddle point. Part of this problem is because we have used a spatially uniform microfield (eq. 5). In reality, the microfield cannot be uniform beyond a distance of about the interparticle separation, and thus under normal conditions, most of the states will be bound. However, for sufficiently high microfields, some excited states will become unbound and this is where resides the problem discussed further in the next sections.

2.2. The Unified Theory of Stark Broadening

In addition to static protons, the absorber also interacts with free electrons. These particles being much faster than the protons, a collisional approach is generally used to describe this interaction. Since the collisions are rapid, the interaction is non-adiabatic and a proper quantum mechanical treatment of the collisions accounting for the internal structure of the hydrogen atom is required. Various theories of Stark broadening for hydrogen lines take into account both the electron and proton interactions (Vidal et al. 1971; Seaton 1990; Stehlé & Jacquemot 1993). Here we summarize the principal aspects of the unified theory of VCS, which even today stands as the most accurate theory for the conditions encountered in white dwarf atmospheres.

The unified theory of VCS uses the quasi-static proton broadening approximation with the distribution of electric microfields described in § 2.1, assumed to be constant in space and time. The complete Stark profile is then defined as

$$S(\alpha) = \int_0^\infty P(\beta) I(\alpha, \beta) d\beta, \quad (9)$$

where $I(\alpha, \beta)$ is the electronic broadening profile. Therefore, the problem is reduced to the calculation of electronic broadening profiles for a fixed microfield of amplitude β . The full broadening profile is then the average of the electronic profiles over all possible microfields weighted by the probability distribution $P(\beta)$. The unified theory is a non-adiabatic quantum mechanical theory that uses the classical path approximation for the electron-absorber interactions, implying that the wave functions are well separable. The interaction potential considers only the first dipole term. The name of the unified theory comes from the fact that the electronic profile is valid at all detunings from the line center. In the asymptotic limit of the line core, the impact approximation is recovered. Furthermore, in the far wings of the lines, the one-electron theory is recovered and the electrons and protons have similar contributions to the broadening.

Now we want to compute the electronic profile for an initial Stark state n_a to a final state n'_a , where this abbreviated notation is used to designate any of the (n, m, q) states. Mostly to reduce the computing time and to simplify the inversion of the matrix involved (see below), the unified theory uses the no-quenching approximation, which means that there are only collision-induced transitions within the same principal level. The states after the collisions will be denoted by n_b and n'_b for the initial and final state, respectively. The calculations can then be performed by considering only two-level transitions. This last approximation is valid only if the difference in energy between the highest Stark state from level n' and the lowest state of level $n' + 1$ is large, or in other words, when the different lines are well separated (i.e., when the line wings do not overlap). Only then is the regime of the linear Stark effect consistent with the basic assumptions of the unified theory.

The electronic broadening profile $I(\alpha, \beta)$ is given by the sum over all states

$$I(\alpha, \beta) = \frac{1}{\pi} \sum_{n_a, n'_a, n_b, n'_b} \rho(n_a) \text{Im} \left[\langle n_a | \vec{d} | n'_a \rangle \langle n'_b | \vec{d} | n_b \rangle \langle n_b | \langle n'_b | \mathcal{K}^{-1}(\alpha, \beta) | n'_a \rangle | n_a \rangle \right], \quad (10)$$

where \vec{d} is the dipole operator, and ρ is the probability that the atom is in the initial state (Boltzmann factor). The operator \mathcal{K} takes into account the linear Stark effect as well as the free electron-atom interactions (see Vidal et al. 1970, eq. XII.2 for more details). Since the operator \mathcal{K} is generally not diagonal in the basis of the (n, m, q) states, it induces a coupling between the various Stark components.

2.3. Non-Ideal Equation of State

One important advance that has provided a better interpretation of the hydrogen lines in DA white dwarfs is a realistic modeling of non-ideal effects at high densities. Bergeron et al. (1991) were the first to include the occupation probability formalism of HM88 to determine the populations of the bound states of hydrogen in white dwarf atmospheres. This probabilistic approach considers the perturbations on each atom by charged and neutral particles. One advantage of this statistical interpretation is that there are no discontinuities in the populations and the opacities when the temperature and the pressure vary, in contrast with other formalisms that simply predict the last bound atomic level under given physical conditions.

Briefly, each atomic level n has a probability w_n of being bound and a probability $1 - w_n$ of being dissociated due to perturbations from other particles in the plasma. The partition function of a given species is then written as

$$Z = \sum_n w_n g_n \exp\left(-\frac{\chi_n}{kT}\right), \quad (11)$$

where χ_n and g_n are respectively the excitation energy and multiplicity of the level. The occupation probability w_n is defined as

$$w_n = \exp\left(-\frac{\partial f / \partial N_n}{kT}\right), \quad (12)$$

where f is the free energy of the non-ideal interaction. The different interactions being statistically independent, the total occupation probability can then be calculated simply as the product of the contributions from neutral and charged particles.

The interaction with neutral particles is treated within a hard sphere model. The configurational free energy is derived from the second virial coefficient in the van de Waals equation of state (excluded volume correction). The exact origin of this excluded volume term is the hard sphere equation of state of Carnahan & Starling (1969). The interaction with charged particles is the one closely related to the Stark effect. This interaction suggests that the electric microfields, fluctuating on long time scales due to changes in the spatial distribution of protons, can destabilize a bound state and cause its dissolution into the continuum. Indeed, we already discussed in § 2.1 that the application of an intense electric field on a bound atom allow for the ionization of the atom. HM88 therefore suggest an occupation probability for proton perturbations of the form

$$w_n(\text{charged}) = \int_0^{\beta_{\text{crit}}} P(\beta) d\beta , \quad (13)$$

where $P(\beta)$ is the probability distribution of the electric microfields introduced in § 2.1. This occupation probability implies that all microfields larger than the critical field β_{crit} will ionize the electrons in level n (it is implicit here that the critical field depends on the atomic level considered). The difficulty with this formulation is to find the value of the critical microfield, for which slightly different expressions can be found in the literature (HM88; Seaton 1990; Stehlé & Jacquemot 1993). The simplest formulation is that of Seaton (1990) which consists in taking the critical microfield as the point where the energy of the highest Stark state for a given level n crosses the energy of the lowest Stark state of the next level $n + 1$. For hydrogen, and using the linear Stark effect, we find

$$\beta_{\text{crit}} = \frac{2n + 1}{6n^4(n + 1)^2} \frac{e}{a_0^2 F_0} . \quad (14)$$

The assumption that the crossing of two atomic levels with different principal quantum numbers leads to the dissolution of the lower level is difficult to prove and it is based in part on laboratory experiments and theoretical considerations (see HM88 for a more detailed discussion). Let us consider one bound electron in one of its many Stark states of the n -th level. When the electric microfield, which fluctuates in time, gets to a value such that there is a *crossing*¹ between this level and the lowest Stark state of the $n + 1$ level, there is a significant probability that when the microfield goes down, there will be a transition $n \rightarrow n + 1$. The incessant fluctuations of the microfield imply that these transitions will continue until the electron becomes unbound. However, the bound electron will in fact be in a rather homogeneous superposition of all its accessible Stark states due to electronic collisions² on time scales much shorter than the fluctuation time for the microfields, and also due to fluctuations in the direction of the microfield. That is, as soon as the first Stark state from a level n crosses another one from the level $n + 1$, the electron is allowed to cascade to the continuum.

The reader might have noticed that equation (14) is based on the linear Stark effect although this is not necessarily a good approximation when levels are crossing. This is why HM88 considered a formulation of the critical field that takes into account corrections

¹Strictly speaking, direct degenerate crossings are avoided due to fine structures and non-uniformity in the microfields.

²See equation 10; the non-diagonal operator \mathcal{K} introduces this coupling.

of higher order from the perturbation theory as well as results from experiments³. They find that for levels with $n > 3$, the linear theory remains valid. For lower levels, however, the critical field is large enough that it must have been created by a single proton very close to the absorber. In this case, the approximation of a uniform electric field in space fails and we must consider the full potential curve of the H_2^+ system to find the critical field (Stehlé & Jacquemot 1993), and also to compute the broadening profiles of the far line wings (Allard & Kielkopf 1982). Exact calculations show that no crossing is possible between levels $n = 1, 2$, and 3 , which implies that $\text{L}\alpha$ is not affected by non-ideal effects due to proton perturbations. Also, the crossing between $n = 3$ and 4 is close to the classical saddle point value, which means that the linear Stark theory is in error by $\sim 14\%$. Therefore, HM88 added a smoothing factor to equation (14) so that the exact result is recovered for $n = 3$. For levels with a high value of n , HM88 obtain the same results as Seaton (1990). For the Balmer lines, these different values of β_{crit} are not an issue since the non-ideal effects discussed above are never important for $\text{H}\alpha$ in DA white dwarfs. This is not the case for $\text{L}\alpha$ and $\text{L}\beta$, however, for which non-ideal effects should be treated with caution, or simply neglected (for instance in TLUSTY and in our code discussed in § 4).

We have seen in § 2.2 that the interaction of hydrogen atoms with rapid electrons was better described with a collisional approach since the quasi-static theory is generally not valid in this case. These perturbations are also considered in the HM88 model. We must keep in mind that because the plasma is in thermal equilibrium, the equation of state already accounts for the inelastic electronic collisions that cause transitions and ionization. However, we expect that if the time between collisions is small, the energy of a bound level will be left undefined by a certain amount given by the uncertainty principle. If this energy uncertainty is of the order of the ionization potential, we expect the state to become unbound after the collision. As stated in HM88, this contribution to the occupation probability is always much lower than the proton contributions and can be neglected in DA atmospheres. However, the electronic perturbations should not be neglected when calculating the line profiles, as discussed in § 3. We must also remember that the electrons contribute indirectly to the occupation probability due to proton perturbations by mixing the Stark states. The occupation probability for the bound states of hydrogen are displayed in Figure 3 for typical conditions encountered at the photosphere of white dwarf stars. Non-ideal effects are shown to be extremely important except for the very lowest transitions. The solution of the HM88 equation of state yields the populations for all states.

Finally, the opacity calculation must also be modified to take into account the occupation

³Remember that even if we have the *exact* critical field, ionization does not necessarily occur exactly at that point and this is why experimental data are also required.

probability formalism, as described by Däppen et al. (1987). The bound-bound (line) opacity for a transition between levels i and j (equation 1) is multiplied by w_j/w_i to take into account the fact that these levels can be dissolved when a photon is absorbed. We thus obtain

$$\kappa_{ij}(\nu) d\nu = N_i \frac{\pi e^2}{m_e} \frac{w_j}{w_i} f_{ij} \phi(\nu) d\nu . \quad (15)$$

When the absorption is from a bound state to a final state that has been dissolved by non-ideal interactions (with a probability $1 - w_j/w_i$), we obtain instead a bound-free opacity since this process is equivalent to the ionization of the atom. We can directly extrapolate, in this case, the bound-free cross section at frequencies below the usual cutoff frequency ν_c . Däppen et al. (1987) have treated this opacity by considering the absorption from a level i of a photon of energy $h\nu$ that yields a transition to a fictitious upper level n^* given by

$$n^* = \left(\frac{1}{n_i^2} - \frac{h\nu}{\chi^I} \right)^{-1/2} . \quad (16)$$

The hydrogen bound-free opacity for $\nu < \nu_c$ — also called the pseudo-continuum opacity — can then be written as

$$\kappa_i(\nu) d\nu = N_i \left(1 - \frac{w_{n^*}}{w_i} \right) \frac{64\pi^4 m_e e^{10}}{3\sqrt{3}ch^6} \frac{g_{bf,i}(\nu)}{n_i^5 \nu^3} d\nu . \quad (17)$$

In Figure 4, we show the individual contributions of the line and pseudo-continuum opacities at the photosphere of a 20,000 K DA white dwarf in the spectral region of the Balmer lines. We can see how the pseudo-continuum opacity extends to wavelengths longward of the Balmer jump, potentially affecting the opacity between the lines, and in particular the high Balmer lines.

3. STARK BROADENING PROFILES INCLUDING NON-IDEAL EFFECTS

The VCS line profiles (§ 2.2) and the HM88 equation of state (§ 2.3) have long been included in modern white dwarf model atmospheres (BSL92; Hubeny & Lanz 1995; Finley et al. 1997; Kawka & Vennes 2006). The HM88 theory has been used, in particular, to calculate populations as well as line and pseudo-continuum opacities. However, all model spectra currently available and calculated within the HM88 framework suffer from a major inconsistency. Seaton (1990) was the first to point out that not only the line strengths will be

affected by non-ideal effects, but the *shape* of the line profiles as well. The Stark broadening profiles $S(\alpha)$ from VCS, for instance, do not take into account such non-ideal effects. It is possible to describe qualitatively the behavior of non-ideal line profiles. The high electric microfields, normally responsible for the absorption in the far wings of the line profiles, will not contribute as much to the line opacity in the non-ideal case since these fields are mostly responsible for dissolving the atomic levels. Consequently, the opacity in the line wings will be significantly reduced with respect to the ideal case. But since by definition the profiles are normalized to unity, the non-ideal line profiles will have deeper cores and appear narrower in comparison with the ideal case.

Instead of including the non-ideal effects discussed above, Bergeron (1993) proposed a solution that could be easily implemented in model atmosphere calculations. As mentioned in the Introduction, this is the solution adopted by BSL92 in their analysis of a large spectroscopic sample of DA stars. The authors found in their preliminary analysis that the atmospheric parameters varied significantly when an increasing number of Balmer lines was included in the fitting procedure. Furthermore, the mean mass of their sample was uncomfortably low ($\langle M \rangle \sim 0.53 M_{\odot}$; Bergeron et al. 1990a). The solution proposed by Bergeron (1993) was to parameterize the value of the critical field in equation (14). The effect of varying the value of β_{crit} is, among other things, to change the relative importance of the line wing and pseudo-continuum opacities. By increasing *arbitrarily* the value of the critical field, one mimics the non-ideal effects by reducing the line wing opacity. One problem with this approach, of course, is that the determination of the multiplicative factor in the expression for β_{crit} has absolutely no physical basis. This factor can only be determined from an empirical analysis of the internal consistency of the fitting procedure, similar to that shown in Figure 2 (see also Bergeron 1993). Furthermore, there is no reason to expect this ad hoc parameter to be the same for all hydrogen levels (i.e., Balmer or Lyman series) or for different atmospheric parameters. Another side effect of this approach is to artificially change the atomic populations in the HM88 equation of state, which in turn could have an unexpected impact on other parts of the model calculations. It should be clear by now that a more physical approach is seriously required, especially given the high quality spectra that have become available in recent years, either in the visible or the ultraviolet. This ad hoc parameter represents an important hurdle towards our understanding of the global properties of white dwarfs.

A coherent way to combine the Stark broadening profiles and the HM88 equation of state is described at length in Seaton (1990). Seaton proposed to replace equation (9) by

$$S(\alpha) = \frac{\int_0^{\beta_{\text{crit}}} P(\beta) I(\alpha, \beta) d\beta}{\int_0^{\beta_{\text{crit}}} P(\beta) d\beta}, \quad (18)$$

where only electric microfields β with an amplitude inferior to the critical field β_{crit} for the upper level of the transition now contribute to the broadening of the lines by the protons. The higher fields contribute instead to the pseudo-continuum opacity. The denominator, which turns out to be the occupation probability due to proton perturbations, allows for the renormalization of the line profiles⁴.

Seaton (1990) was the first to calculate Stark broadening profiles taking into account non-ideal effects. However, his calculations made for the Opacity Project rely on an approximate electron broadening theory that is inappropriate in the context of white dwarf atmospheres. Stehlé & Jacquemot (1993) also discuss the implementation of non-ideal effects inside the line profile calculations using an alternative electron broadening theory. This theory also lifts in part the static approximation for the protons and therefore gives better results in the center of the profiles, but this has no effect on the spectrum at the high densities found in white dwarf atmospheres. In the line wings, the results are equivalent to the VCS formulation. We must mention, however, that all published tables and subsequent papers for this theory (Stehlé 1994; Stehlé & Hutcheon 1999) do not include non-ideal effects.

In this work, we use the Seaton approach (equation 18) to include non-ideal effects due to proton perturbations inside the unified theory of Stark broadening from VCS. We also include non-ideal corrections due to electronic perturbations according to the HM88 theory. This was neglected by Seaton (1990), likely because it was estimated that the effects would be negligible in the context studied. As discussed in § 2.3, the collisions between free electrons and the absorber leave a bound level in a state of indefinite energy. Therefore, the HM88 model states that if the uncertainty on the energy becomes equal to the ionization energy of the level, the electron has a good probability of becoming unbound. Here we have at hand the electronic broadening profiles given by equation (10), and their wings generally extend to infinity in terms of the detuning $\Delta\nu$ (measured from the line center). However, according to the HM88 theory, it is obvious that the detuning induced by the electronic collisions cannot extend much beyond ν_c (i.e. the ionization threshold frequency for this level) or there would be line opacity shortward of the Balmer or Lyman jumps. An abrupt

⁴In the definition of Seaton (1990), the line profiles are not renormalized but instead the factor w_j is omitted in equation 15.

cutoff is not desirable since this could cause discontinuities in the spectra. We adopt here an exponential cutoff so that the electronic broadening profiles are reduced by a factor of e^{-1} at $\Delta\nu = \nu_c - \nu_0$, where ν_0 is the central frequency of the transition, and then we renormalize the total broadening profiles. Since the exponential factor is independent of β , we can easily represent this correction in the form

$$\phi'(\nu) = \frac{\phi(\nu)e^{-|\nu-\nu_0|/\nu_c}}{\int_0^\infty \phi(\nu)e^{-|\nu-\nu_0|/\nu_c} d\nu} . \quad (19)$$

This has a small but non-negligible effect on the line wings, especially for the higher members of the series. Both T_{eff} and $\log g$ are increased by $\sim 0.5\%$ when this correction is introduced in our calculations. Using alternative types of cutoff, we estimate that the uncertainties on this part of the theory can be as high as half of the shifts found here. As mentioned in HM88, a more physical approach is certainly much needed but such a theory still does not exist.

Figure 5 presents the Stark broadening profiles $S(\alpha)$ for the Balmer lines H γ and H8 at typical photospheric conditions of DA stars. Along with the results from this work, we show the original calculations of VCS (Lemke 1997) and the approximate profiles from Seaton (1990). We note that our profiles including non-ideal effects due to proton and electron perturbations are very different from the original ideal gas calculations of VCS, even though we are using the same broadening theory. Our profiles have significantly less opacity in the line wings, and higher lines of the series have much sharper profiles, as anticipated. To have a better idea of the relative importance of the two improvements discussed above, we have estimated that the electronic corrections account for 12% and 16% of the reduction of the opacity at 100 Å from the line center of H γ and H8, respectively. Finally, we show that our profiles are not in agreement with the calculations of Seaton (1990), which include non-ideal effects due to proton perturbations but use only an approximate treatment for the electronic broadening. These results confirm that this last approximation is not suitable for typical conditions encountered in DA white dwarf atmospheres. The comparison of our Lyman line profiles with the calculations of VCS or Seaton is similar to those displayed in Figure 5.

We have demonstrated in the previous sections that our approach to Stark broadening provides significant physical improvements over previously available calculations. When included in a model atmosphere, the equation of state and the opacity calculations become entirely consistent without the need of the ad hoc parameter introduced by Bergeron (1993). By including non-ideal effects, we have shown that the line profiles from the unified theory are dramatically modified in typical white dwarf atmospheres. These improved profiles now

need to be validated using spectroscopic data.

3.1. Comparison with Laboratory Experiments

The preferred way to validate Stark broadening theories for hydrogen has been the comparison with laboratory plasma emissivity measurements from Wiese et al. (1972). These pure hydrogen plasma arc experiments were performed at high densities and temperatures, comparable to the photospheric conditions of cool white dwarfs. The main advantage of this experiment is that it is not under the constraint of radiative equilibrium, unlike a stellar atmosphere. In other words, the emergent flux at one wavelength is not affected by what occurs at other wavelengths. The emissivity can then be simply written as

$$j_{\lambda}(\lambda) = \frac{2c}{\lambda^4} \kappa(\lambda) e^{-hc/\lambda kT} , \quad (20)$$

where $\kappa(\lambda)$ represents the total monochromatic opacity. Another advantage, at least from a theoretical point of view, is that it is easier to control the experiments and the results are independent of various sources of uncertainty intrinsic to DA model atmospheres (i.e., convection, contamination from heavy elements, etc.). We use the data for the lowest and highest density experiments (the most extreme positions on the plasma arc) from Wiese et al., which were compared to broadening theories in various studies (Däppen et al. 1987; Seaton 1990; Bergeron 1993; Stehlé & Jacquemot 1993). Wiese et al. estimate the LTE plasma parameters for these two experiments at $\log T = 4.00$, $\log N_e = 16.26$ and $\log T = 4.12$, $\log N_e = 16.97$, respectively. However, there is no simple way to measure the plasma state parameters and it is not clear whether LTE is reached or not. The authors used the total intensity from two lines, together with the intensity at two continuum points, and fitted the data with an approximate plasma model. Since then, slightly different parameters have been used to compare with broadening theories. Instead of choosing approximate values for the parameters like in previous analyses, we performed a χ^2 fit to the full data sets, using the same input physics as for our white dwarf models. The results with the original VCS calculations and our improved line profiles are displayed in Figures 6 and 7 in terms of absolute predicted fluxes (i.e., without any renormalization).

For the lower density experiment of Figure 6, our improved profiles provide a much better fit to the laboratory data, in particular in the regions of the high Balmer lines where the wings overlap. The higher density experiment of Figure 7 is more problematic. We find that there is a partial $T - N_e$ degeneracy in the χ^2 diagram; it is indeed possible to find many acceptable solutions from visual inspection by increasing both T and N_e . However,

to provide the best overall fit with our new profiles, we have to increase the plasma state parameters significantly compared to the Wiese et al. values. We see that our profiles provide the best fit for the higher lines, although the red wings of $H\beta$ and $H\gamma$ are predicted a bit too weak. All in all, we conclude that the experiments of Wiese et al. do not provide such a stringent constraint on the broadening theories because of the large range of acceptable plasma state parameters, and also because of potential departures from LTE.

3.2. Further Theoretical Improvements

While our work represents a significant advance over previous calculations, second order effects in the theory of Stark broadening could still come into play. Such second order effects have been studied extensively in the literature in the case of high density hydrogen plasma experiments (Lee & Oks 1998; Stehlé et al. 2000; Demura et al. 2008). The sources of these second order effects are plentiful but they all have the same impact on the line profiles: they produce asymmetries and they shift the central wavelengths, the latter being unimportant for the spectroscopic technique used to measure the atmospheric parameters of white dwarfs. The recent study of Demura et al. (2008) reveals that the various second order effects compete and interact together in a complex way and that they should all be included in the models simultaneously. The most important effects are due to quadrupole proton-absorber interactions and to the quadratic Stark effect, but second order effects due to quadrupole electron-absorber interactions are noticeable as well. The lifting of the no-quenching approximation could also be considered a second order effect, although it was shown by Lee & Oks (1998) to have an impact mostly on the line cores. Furthermore, some of these quenching effects have already been accounted for implicitly by including here the HM88 non-ideal effects directly inside the line profile calculations. Finally, even if we include better physics for the atomic transitions, we still have to rely on the HM88 equation of state, which is, or may become, the main source of uncertainty.

Our analysis above of the Wiese et al. experiments, with our improved profiles has already revealed the existence of line profile asymmetries. For the lower density experiment (see Fig. 6), it is only a mild effect in the far wings, however. It is not clear if such second order effects would be significant in a typical DA white dwarf at $\log g \sim 8$, for which the electronic density at the photosphere is roughly halfway between the two Wiese et al. experiments. Therefore, it is probably premature at this stage to include second order effects in our calculations, and it is not clear whether such changes would affect our line profiles significantly. We come back to this point in the analysis of the PG spectroscopic sample discussed below.

4. APPLICATION TO WHITE DWARF ATMOSPHERES

4.1. Model Spectra

We now discuss the astrophysical implications of our improved line profiles described in § 3 on the modeling of DA white dwarfs. Our model atmosphere code is based on the program originally developed by Bergeron et al. (1991, 1995a) and references therein. The main difference is that we have updated several sources of opacity and partition functions (all within the occupation probability formalism). For completeness, we provide in Table 1 the complete list of opacity sources included in our code. We have not included the $L\alpha$ line broadening due to H_2 collisions (Kowalski & Saumon 2006) since these calculations are still not available, although this has no impact over the range of effective temperature considered here.

We restrain our analysis to effective temperatures above $\sim 13,000$ K to avoid additional uncertainties related to convective energy transport. Indeed, the atmospheric structure of DA white dwarfs below this temperature depends sensitively on the assumed convective efficiency. The most commonly used approach to include convection in model atmosphere calculations, the mixing-length theory, is at best a very crude approximation, and the convective efficiency must be parameterized by carefully adjusting the value of the mixing length (Bergeron et al. 1995b). It is also believed that large amounts of helium can be brought to the surface by convection while remaining spectroscopically invisible (Bergeron et al. 1990b; Tremblay & Bergeron 2008). Hence, it is not even clear whether cool DA stars have hydrogen-rich atmospheres. Another reason for restricting our analysis to hotter stars is that neutral line broadening becomes important for the Balmer lines below $T_{\text{eff}} \sim 10,000$ K, preventing us from performing a direct comparison of the observed and predicted Stark broadened absorption lines. We also set an upper limit of $T_{\text{eff}} = 40,000$ K because NLTE effects become important above this temperature. Also, absorption from heavier elements, particularly in the UV, is likely to affect the atmospheric structure of hot white dwarfs.

We thus computed two grids of model atmospheres, one with the VCS profiles and the other with our improved profiles (both calculated with $\beta_{\text{crit}} \times 1$), covering the range of $T_{\text{eff}} = 12,000$ K to 45,000 K (with steps of 500 K up to 15,000 K, 1000 K up to 18,000 K, 2000 K up to 30,000 K, and 5000 K above) and of $\log g = 6.5$ to 9.5 (by steps of 0.5 dex with additional models at 7.75 and 8.25). To compare the model spectra calculated from both sets of line profiles, we simply fit the VCS spectra with our improved spectra. The results of this exercise are illustrated in Figure 8. In general, our new models yield systematically higher effective temperatures (by 1000 – 2000 K) and surface gravities (by ~ 0.1 dex) over the entire range of atmospheric parameters considered here. One exception is a region at

low temperatures and high surface gravities where the trend in temperature is reversed. The strip, inclined in the diagram near $T_{\text{eff}} \sim 15,000$ K, where this separation occurs corresponds to the region where the strength of the Balmer lines reaches its maximum (Bergeron et al. 1995b). Our new models predict Balmer lines that are stronger, hence the temperatures in this region are pushed towards lower values.

4.2. Analysis of the DA Stars in the PG Sample

In this section, we measure the implications of our improved Stark profiles on the analysis of Balmer line observations of DA stars by considering the Palomar-Green sample of Liebert et al. (2005). This sample of 348 DA stars has been studied in great detail, and the range of effective temperatures for these objects corresponds very well to that considered in our analysis. About 250 white dwarfs fall in the appropriate range of T_{eff} , depending on which model grid is used. The data set and the fitting procedure of the optical spectra are identical to those described at length in Liebert et al. (2005, and references therein). Briefly, we first normalize the observed and model flux from each line to a continuum set to unity at a fixed distance from the line center. The observed profiles are then compared with the predicted profiles, convolved with a Gaussian instrumental profile. The atmospheric parameters are then obtained using the non-linear least-squared method of Levenberg-Marquardt, fitting simultaneously five lines ($H\beta$ to $H8$). In some cases where the spectrum is contaminated by a M dwarf companion, one or two lines are excluded from the fit.

As discussed in the Introduction, model spectra calculated with standard Stark broadening profiles yield inconsistent atmospheric parameters when different lines are included in the fitting procedure. As shown in the bottom panel of Figure 2, our improved Stark profiles provide an even better internal consistency than the previous calculations displayed in the two upper panels. To better quantify this internal consistency, we perform for each star in the PG sample the same exercise as that shown in Figure 2 using the VCS profiles and our improved profiles. We then compute for the 250 stars in our sample the average absolute deviations in T_{eff} and $\log g$ between the solutions obtained with a different number of lines included in the fit. The results of this exercise are presented as filled circles in Figure 9 together with the mean uncertainties from the fitting procedure as a reference point (the open circles will be discussed in § 4.3). We can see that the deviations with our improved profiles have been significantly reduced by a factor of ~ 1.6 in T_{eff} and ~ 1.8 in $\log g$. Furthermore, these deviations now both lie within the mean uncertainties of the fitting procedure, a result which is extremely reassuring.

The quality of the fits is also an important aspect of the comparison between model

grids. We compare in Figure 10 our best fit to WD 0205+250 (same star as in Fig. 2) using the VCS profiles and our improved Stark profiles. This comparison reveals that while the atmospheric parameters are significantly different, the quality of the fits is similar. We thus conclude that the quality of the fits cannot help to discriminate between both sets of Stark profiles.

We can also explore the global properties of the PG sample with our two model grids. We first convert the $\log g$ values into mass using evolutionary models appropriate for white dwarfs with thick hydrogen layers (see Liebert et al. 2005 for details). Our results are presented in Figure 11 in a mass versus effective temperature diagram. As expected from the previous comparison displayed in Figure 10, our improved line profiles yield significantly larger masses and higher effective temperatures. We note that the results displayed in the bottom panel are qualitatively similar to the early spectroscopic determination of the mass distribution of DA stars by Bergeron et al. (1990a), which was based on the VCS profiles without any modification of the critical field. In this case, the mass distribution has a mean value near $0.53 M_{\odot}$, which is uncomfortably low compared to what is expected from earlier phases of stellar evolution (see the discussion in Bergeron et al. 1990a).

Finally, we have also investigated whether second order effects in the Stark broadening theory, such as those discussed in § 3.2, could be detected in our analysis. In particular, if such effects are present, we would expect to observe differences in the fits of the blue and red wings of the Balmer lines. We have thus reanalyzed the PG sample by including in the fit (1) only the red wing of the Balmer lines and (2) only the lines cores (this is accomplished by fitting only half of the wavelength range we normally use for each line). We find that the atmospheric parameters obtained in this manner are entirely consistent, and we thus conclude that second order effects can be safely neglected in DA white dwarfs.

4.3. A Reappraisal of Previous Studies of DA White Dwarfs

The spectroscopic determination of the mass distribution by BSL92 was based on model spectra that include the solution proposed by Bergeron (1993) to mimic the non-ideal effects, namely by taking twice the value of the critical field ($\beta_{\text{crit}} \times 2$) in the HM88 formalism. This ad hoc procedure had the effect of artificially reducing the pseudo-continuum opacity, and thus the opacity in the wings of the high Balmer lines. The internal consistency of the solutions obtained from different lines was consequently improved, as can be judged from the results displayed in Figures 2 and 9 (open circles). Since this ad hoc solution has been adopted by BSL92 and in all white dwarf models used in the literature, it is important to evaluate the differences between our revised atmospheric parameters and those published

in the literature based on these approximate model spectra. For this purpose, we have also calculated another model atmosphere grid using the original VCS profiles from Lemke (1997) but with twice the value of the critical field. This grid is similar to that used by the Montreal group in the past ten years or so, and which has been applied to several studies of DA white dwarfs using the spectroscopic technique.

Once again, we rely on the PG sample of DA stars analyzed above. A comparison similar to that shown in Figure 11 is not very instructive here since the differences in T_{eff} and $\log g$ are considerably smaller. Instead, we use the representation displayed in Figure 12 where the differences ΔT_{eff} and $\Delta \log g$ are shown as a function of effective temperature. This comparison reveals that our improved line profiles yield higher effective temperatures and surface gravities, with an important correlation with T_{eff} . In particular, the $\log g$ values are about 0.05 dex larger above 20,000 K but can be as much as 0.1 dex larger near 15,000 K. Similarly, the differences in temperatures reach a maximum near 25,000 K but decrease at both lower and higher effective temperatures. The corresponding mass distributions, displayed in Figure 13, indicate that the mean mass is shifted by $+0.034 M_{\odot}$ when our new models are used. The shape of the mass distributions is statistically equivalent, however, and the dispersion remains the same. We must also point out that according to the results of Tremblay & Bergeron (2008), 15% of the DA white dwarfs in the temperature range considered here probably have thin hydrogen layers ($M_{\text{H}}/M_{\text{tot}} < 10^{-8}$). Consequently, the typical values for the mean mass are probably ~ 0.005 to $0.01 M_{\odot}$ lower than the values reported in Figure 13.

As discussed in the Introduction, the spectroscopic technique provides very accurate measurements of the atmospheric parameters, allowing for a relative comparison of these parameters among individual stars. However, the *absolute* values of the atmospheric parameters may suffer from an offset due to uncertainties in the physics included in the model calculations. Hence it is very important to compare the results with independent methods. The most reliable independent observational constraint for DA white dwarfs comes from trigonometric parallax measurements. Holberg et al. (2008a) have shown using the recent photometric calibrations of Holberg & Bergeron (2006) that there exists a very good correlation between spectroscopically based photometric distance estimates and those derived from trigonometric parallaxes. Here we compare absolute visual magnitudes instead of distances. We first combine trigonometric parallax measurements with V magnitudes to derive $M_V(\pi)$ values. We then use the calibration of Holberg & Bergeron (2006) to obtain $M_V(\text{spec})$ from spectroscopic measurements of T_{eff} and $\log g$. We selected 92 DA stars with known parallaxes from the sample of Bergeron et al. (2007) (the uncertainties on the parallaxes must be less than 30%). The M_V values obtained from both model grids described in this section are compared in Figure 14. The agreement is very good within the parallax uncertainties for

both model grids. Hence, despite the fact that our new models yield higher values of T_{eff} and $\log g$ (i.e., smaller radii), these two effects almost cancel each other and the predicted luminosities (or M_V) remain unchanged, and so are the conclusions of Holberg et al. (2008a). Another important constraint is provided by the bright white dwarf 40 Eri B for which a very precise trigonometric parallax and visual magnitude have been measured by Hipparcos. These measurements yield $M_V = 11.01 \pm 0.01$, while we predict $M_V = 11.02 \pm 0.07$ and 10.97 ± 0.07 based on our new and VCS models, respectively. Although both determinations agree within the uncertainties with the observed value, our new grid provides an exact match to the measured M_V value.

We also point out that trigonometric parallax measurements are available mostly for cool white dwarfs (Bergeron et al. 1997) and nearby white dwarfs (Holberg et al. 2008b), which are excluded from our analysis. In contrast with our approach here, Bergeron et al. (1997) and Holberg et al. (2008b) make use of photometric measurements that cover the full spectral energy distributions, and both studies find mean masses near 0.65-0.66 M_{\odot} , consistent with our spectroscopic determinations for the PG sample.

5. CONCLUSION

We have combined for the first time in a consistent physical framework the unified theory of Stark broadening from Vidal, Cooper, & Smith and the HM88 non-ideal equation of state. Both of these well known theories represent the basis of our current knowledge of DA white dwarfs. Following the suggestion of the late Mike Seaton, we have taken into account the non-ideal effects due to proton and electron perturbations directly into the line profile calculations. We have shown that our improved line profiles are significantly different from other Stark profiles that have been used in previous studies. We have computed the first grid of model spectra without the need of the parameterization of the critical field introduced by Bergeron (1993) and used in *all* previous models to mimic these non-ideal effects. We have demonstrated that our new profiles have important astrophysical implications. In particular, the mean mass of DA white dwarfs is $\sim 0.03 M_{\odot}$ higher than previously measured. Yet, our updated atmospheric parameters determined from the spectroscopic technique remain in excellent agreement with the constraints imposed by trigonometric parallax measurements.

Future work will confront our improved models with observations in the more complex regime of higher and lower effective temperatures. An exhaustive look at the Lyman line analysis of UV observations from FUSE is also much needed since the model spectra are highly sensitive to the non-ideal effects in that particular spectral region. For cooler white dwarfs, we must also investigate the abrupt cut-off that has been introduced to limit the

effects of the Lyman pseudo-continuum opacity.

We thank A. Gianninas for a careful reading of our manuscript, and M. Lemke for providing us with his computer version of the VCS code. We also thank the two referees for their constructive comments, which have greatly helped improving the presentation of our results. This work was supported in part by the NSERC Canada and by the Fund FQRNT (Québec). P. Bergeron is a Cottrell Scholar of Research Corporation for Science Advancement.

REFERENCES

- Ali, A. W., & Griem, H. R. 1965, *Physical Review*, 140, 1044
- Ali, A. W., & Griem, H. R. 1966, *Physical Review*, 144, 366
- Allard, N., & Kielkopf, J. 1982, *Reviews of Modern Physics*, 54, 1103
- Allard, N. F., Kielkopf, J. F., & Loeillet, B. 2004, *A&A*, 424, 347
- Barstow, M. A., Good, S. A., Burleigh, M. R., Hubeny, I., Holberg, J. B., & Levan, A. J. 2003, *MNRAS*, 344, 562
- Bell, K. L. 1980, *Journal of Physics B Atomic Molecular Physics*, 13, 1859
- Bergeron, P. 1993, *NATO ASIC Proc. 403: White Dwarfs: Advances in Observation and Theory*, 267
- Bergeron, P., Gianninas, A., & Boudreault, S. 2007, in *Proc. 15th European Workshop on White Dwarfs*, ed. R. Napiwotzki & M. Burleigh (San Francisco: ASP), 372, 29
- Bergeron, P., Leggett, S. K., & Ruiz, M. T. 2001, *ApJS*, 133, 413
- Bergeron, P., Ruiz, M. T., & Leggett, S. K. 1997, *ApJS*, 108, 339
- Bergeron, P., Saffer, R. A., & Liebert, J. 1990a, in *Confrontation between Stellar Pulsation and Evolution*, ed. C. Cacciari, A. S. P. Conference Series (Astronomical Society of the Pacific : Provo, Utah), 513
- Bergeron, P., Saffer, R. A., & Liebert, J. 1992, *ApJ*, 394, 228 (BSL92)
- Bergeron, P., Saumon, D., & Wesemael, F. 1995a, *ApJ*, 443, 764
- Bergeron, P., Wesemael, F., & Fontaine, G. 1991, *ApJ*, 367, 253
- Bergeron, P., Wesemael, F., Fontaine, G., & Liebert, J. 1990b, *ApJ*, 351, L21
- Bergeron, P., Wesemael, F., Lamontagne, R., Fontaine, G., Saffer, R. A., & Allard, N. F. 1995b, *ApJ*, 449, 258
- Borysow, U. G., Jorgensen, A. & Fu, Y. 1991, *J. Quant. Spec. Radiat. Transf.*, 68, 235
- Carnahan, N. F., & Starling, K. E. 1969, *J. Chem. Phys.*, 51, 635
- Condon, E. U., & Shortley, G. H. 1935, *The Theory of Atomic Spectra* (Cambridge: University Press)

- Dalgarno, A., & Williams, D. A. 1962, *ApJ*, 136, 690
- Däppen, W., Anderson, L., & Mihalas, D. 1987, *ApJ*, 319, 195
- Demura, A. V., Demchenko, G. V., & Nikolić, D. 2008, *European Physical Journal D*, 46, 203
- Edmonds, F. N., Jr., Schluter, H., & Wells, D. C. 1967, *MmRAS*, 71, 271
- Eisenstein, D. J., et al. 2006, *ApJS*, 167, 40
- Finley, D. S., Koester, D., & Basri, G. 1997, *ApJ*, 488, 375
- Friedrich, H. 2006, *Theoretical Atomic Physics* (3d ed., Berlin: Springer)
- Gianninas, A., Bergeron, P., & Dufour, P. 2005, in *ASP Conf. Ser. 334, 14th European Workshop on White Dwarfs*, ed. D. Koester & S. Moehler (San Francisco: ASP), 139
- Gianninas, A., Bergeron, P., & Fontaine, G. 2006, *AJ*, 132, 831
- Gustafsson, M., & Frommhold, L. 2003, *A&A*, 400, 1161
- Hammond, G. L., Sion, E. M., Kenyon, S. J., & Aannestad, P. A. 1991, in *7th European Workshop on White Dwarfs, NATO ASI Series*, ed. G. Vauclair & E. M. Sion (Dordrecht: Kluwer Academic Publishers), 317
- Holberg, J. B., & Bergeron, P. 2006, *ApJ*, 132, 1221
- Holberg, J. B., Bergeron, P., & Gianninas, A. 2008a, *AJ*, 135, 1239
- Holberg, J. B., Sion, E. M., Oswalt, T., McCook, G. P., Foran, S., & Subasavage, J. P. 2008b, *AJ*, 135, 1225
- Hooper, C. F. 1968, *Physical Review*, 169, 193
- Hubeny, I., & Lanz, T. 1995, *ApJ*, 439, 875
- Hummer, D. G., & Mihalas, D. 1988, *ApJ*, 331, 794 (HM88)
- John, T. L. 1988, *A&A*, 193, 189
- Kawka, A., & Vennes, S. 2006, *ApJ*, 643, 402
- Kepler, S. O., Kleinman, S. J., Nitta, A., Koester, D., Castanheira, B. G., Giovannini, O., Costa, A. F. M., & Althaus, L. 2007, *MNRAS*, 375, 1315

- Kissel, L. 2000, *Radiation Physics and Chemistry*, 59, 185
- Kowalski, P. M., & Saumon, D. 2006, *ApJ*, 651, L137
- Kurucz, R. L. 1970, *SAO Special Report*, 309,
- Lee, R. W., & Oks, E. 1998, *Phys. Rev. E*, 58, 2441
- Lemke, M. 1997, *A&AS*, 122, 285
- Liebert, J., Bergeron, P., & Holberg, J. B. 2005, *ApJS*, 156, 47
- Mihalas, D. 1978, *Stellar Atmospheres* (2nd ed., San Francisco: Freeman)
- Nayfonov, A., Däppen, W., Hummer, D. G., & Mihalas, D. 1999, *ApJ*, 526, 451
- Seaton, M. J. 1990, *Journal of Physics B Atomic Molecular Physics*, 23, 3255
- Smith, E. W., Cooper, J., & Vidal, C. R. 1969, *Physical Review*, 185, 140
- Stehlé, C. 1994, *A&AS*, 104, 509
- Stehlé, C., Gilles, D., & Demura, A. V. 2000, *European Physical Journal D*, 12, 355
- Stehlé, C., & Hutcheon, R. 1999, *A&AS*, 140, 93
- Stehlé, C., & Jacquemot, S. 1993, *A&A*, 271, 348
- Tremblay, P.-E., & Bergeron, P. 2008, *ApJ*, 672, 1144
- Underhill, A. & Waddell, J. 1959, *Stark Broadening Functions for the Hydrogen Lines* (Washington, D.C.: U.S. Dept. of Commerce)
- Vennes, S., Chayer, P., Dupuis, J., & Lanz, T. 2005, in *ASP Conf. Ser. 334, 14th European Workshop on White Dwarfs*, ed. D. Koester & S. Moehler (San Francisco: ASP), 185
- Vidal, C. R., Cooper, J., & Smith, E. W. 1970, *Journal of Quantitative Spectroscopy and Radiative Transfer*, 10, 1011 (VCS)
- Vidal, C. R., Cooper, J., & Smith, E. W. 1971, *Journal of Quantitative Spectroscopy and Radiative Transfer*, 11, 263
- Vidal, C. R., Cooper, J., & Smith, E. W. 1973, *ApJS*, 25, 37
- Wegner, G., & Schulz, H. 1981, *A&AS*, 43, 473

Wesemael, F., van Horn, H. M., Savedoff, M. P., & Auer, L. H. 1980, ApJS, 43, 159

Wiese, W. L., Kelleher, D. E., & Paquette, D. R. 1972, Phys. Rev. A, 6, 1132

Table 1. Opacity Sources Included

Opacity	Populations	Cross Section
H bound-bound, Stark broadening (H–H ⁺ , H–e [−])	N _i (H)	This work
H bound-bound, quasi-molecular (H–H, H–H ⁺)	N(H)	Allard et al. (2004)
H bound-bound, neutral broadening (H–H)	N _i (H)	Ali & Griem (1965, 1966)
H bound-free	N _i (H)	Mihalas (1978)
H free-free	N _e N(H ⁺)	Mihalas (1978)
H ₂ free-free	N _e N(H ₂ ⁺)	we assume that of H I
H ₃ free-free	N _e N(H ₃ ⁺)	we assume that of H I
H [−] bound-free	N(H [−])	John (1988)
H [−] free-free	N _e N(H)	John (1988)
H ₂ ⁺ bound-free	N(H ₂ ⁺)	Kurucz (1970)
H ₂ ⁺ free-free	N(H)N(H ⁺)	Kurucz (1970)
H ₂ [−] free-free	N _e N(H ₂)	Bell (1980)
CIA H–H ₂	N(H)N(H ₂)	Gustafsson & Frommhold (2003)
CIA H ₂ –H ₂	N(H ₂)N(H ₂)	Borysow et al. (2001)
Rayleigh H	N(H)	Kissel (2000)
Rayleigh H ₂	N(H ₂)	Dalgarno & Williams (1962)
Thompson <i>e</i> scattering	N _e	Mihalas (1978)

Note. — The bound-bound H₂ and H₃⁺ opacities are always negligible in DA white dwarfs.

Fig. 1.— Theoretical line profiles of models at different effective temperatures and surface gravities using our new line profiles discussed in § 3. The lines correspond to H β to H8 (*bottom to top*) from the Balmer series of the hydrogen atom. In each panel, the line profiles range from $\log g = 7.0$ (*dashed line*) to 9.0 (*thick line*) by steps of 0.5 dex. The profiles have been convolved with a 6 Å FWHM Gaussian profile, normalized to a continuum set to unity, and offset vertically from each other for clarity.

Fig. 2.— Solutions in a $T_{\text{eff}} - \log g$ diagram for a typical DA star using 1 line (H β), 2, 3, 4 and 5 lines (up to H8) in the fitting procedure (represented by thicker 1σ uncertainty ellipses from our fitting procedure). The top panel shows the results with the VCS line profiles, while the middle panel also includes the ad hoc parameter proposed by Bergeron (1993). The bottom panel is with our new line profiles discussed in this work (§ 3).

Fig. 3.— Total occupation probability w_n for the bound states of hydrogen with principal quantum number n for $T = 10,000$ K, $\log N_e = 17$ (*filled circles*) and $T = 20,000$ K, $\log N_e = 16$ (*open circles*).

Fig. 4.— Atomic hydrogen opacity at the photosphere of a 20,000 K DA white dwarf. The contributions of line and pseudo-continuum opacities are shown as solid and dotted lines, respectively.

Fig. 5.— Stark broadening profiles as a function of wavelength measured from the line center at $T = 10,000$ K and $\log N_e = 17$. Results are shown for H γ (*left*) and H8 (*right*). In each panel, we compare the results from this work (based on the VCS theory coupled with non-ideal effects from HM88; *solid lines*) with the original VCS calculations (*dashed lines*). Also shown are the approximate calculations of Seaton (1990, *dotted lines*), which also include non-ideal effects.

Fig. 6.— Emissivity of a hydrogen plasma (*filled dots*) for the low-density experiment of Wiese et al. (1972). Our best fits (*solid line*) to the data are shown for different line broadening theories identified at the top of each panel along with the plasma state parameters obtained from the minimization procedure.

Fig. 7.— Same as Figure 6 but with the data set for the high-density experiment of Wiese et al. (1972).

Fig. 8.— Corrections that must be applied to transform the atmospheric parameters obtained from the VCS profiles to our improved models. These have been obtained by simply fitting the Balmer line profiles of the VCS model grid with our new spectra. For clarity, we have omitted the grid points at $\log g = 7.75$ and 8.25.

Fig. 9.— *Left:* For each star in the PG sample with $40,000 \text{ K} > T_{\text{eff}} > 13,000 \text{ K}$, we computed the average absolute deviation in T_{eff} between solutions obtained from fits that include 2 to 5 lines (similar to Fig. 2). These deviations were then averaged for all DA stars in our sample (*filled dots*). The results are shown for the three grids discussed in the text and identified on the x -axis. For comparison, the mean uncertainty of the fitting procedure is shown as dotted lines. *Right:* Same as left panel but for the dispersion in $\log g$.

Fig. 10.— Our best fit to the Balmer lines of WD 0205+250 with our improved line profiles (*left panel*) and with the VCS profiles (*right panel*). The atmospheric parameters are given in each panel.

Fig. 11.— Mass versus T_{eff} distribution for the DA stars in the PG sample in the range $40,000 \text{ K} > T_{\text{eff}} > 13,000 \text{ K}$. Results are shown for both our improved lines profiles (*top panel*) and the VCS profiles (*bottom panel*). Lines of constant mass at 0.55 and $0.70 M_{\odot}$ are shown as a reference.

Fig. 12.— Differences in T_{eff} and $\log g$ obtained with our improved models and with the VCS profiles ($\beta_{\text{crit}} \times 2$) as a function of effective temperature for the DA stars in the PG sample in the range $40,000 \text{ K} > T_{\text{eff}} > 13,000 \text{ K}$. The solid lines represent the 1:1 correlation while the dotted lines correspond to the uncertainties of the spectroscopic method as determined by Liebert et al. (2005).

Fig. 13.— Mass distributions for the subsample of PG stars studied in Figure 12. The mean masses are reported in the figure.

Fig. 14.— Comparison of the absolute visual magnitudes obtained from trigonometric parallax measurements and from the spectroscopic technique using both model grids. The analysis is restricted to $40,000 \text{ K} > T_{\text{eff}} > 13,000 \text{ K}$. The error bars represent the average uncertainties. WD 1606+422 (*open circle*) is a suspected double degenerate binary (Bergeron et al. 2001).

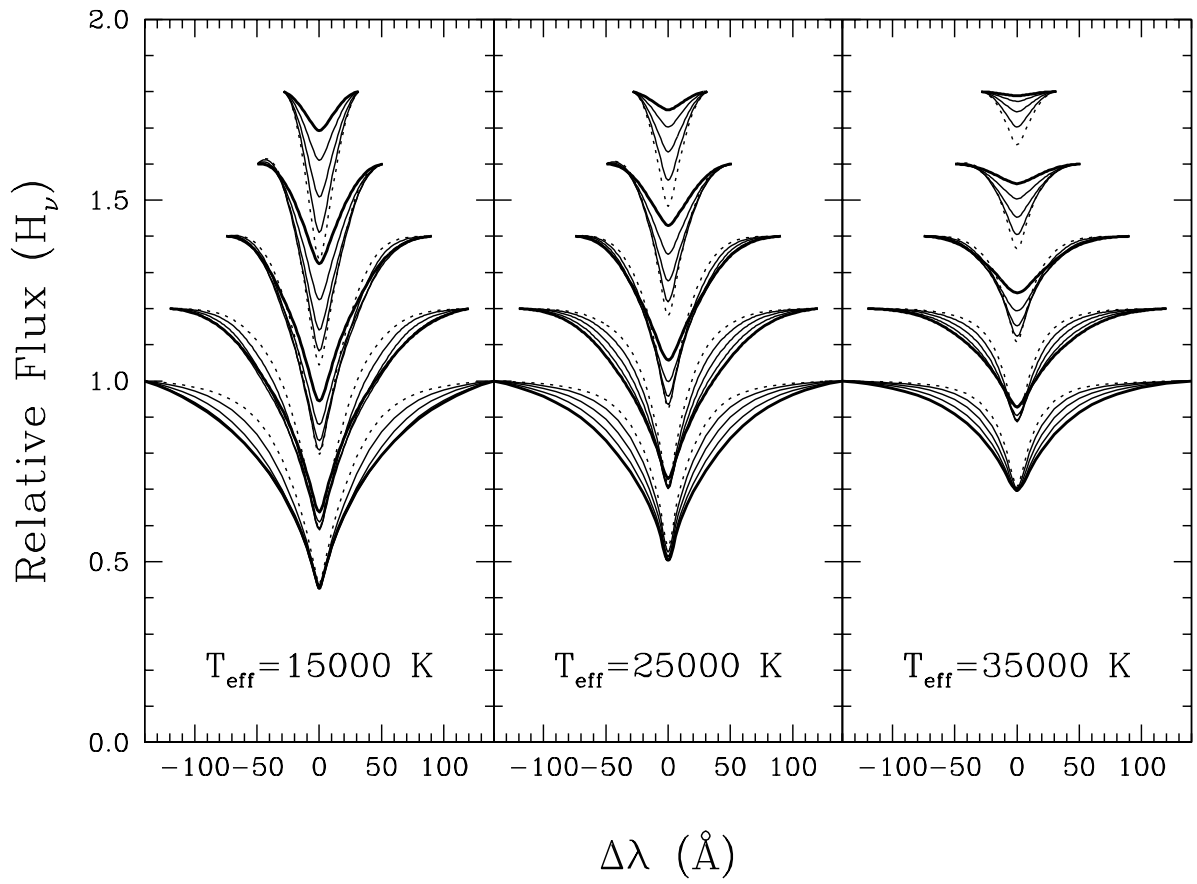


Figure 1

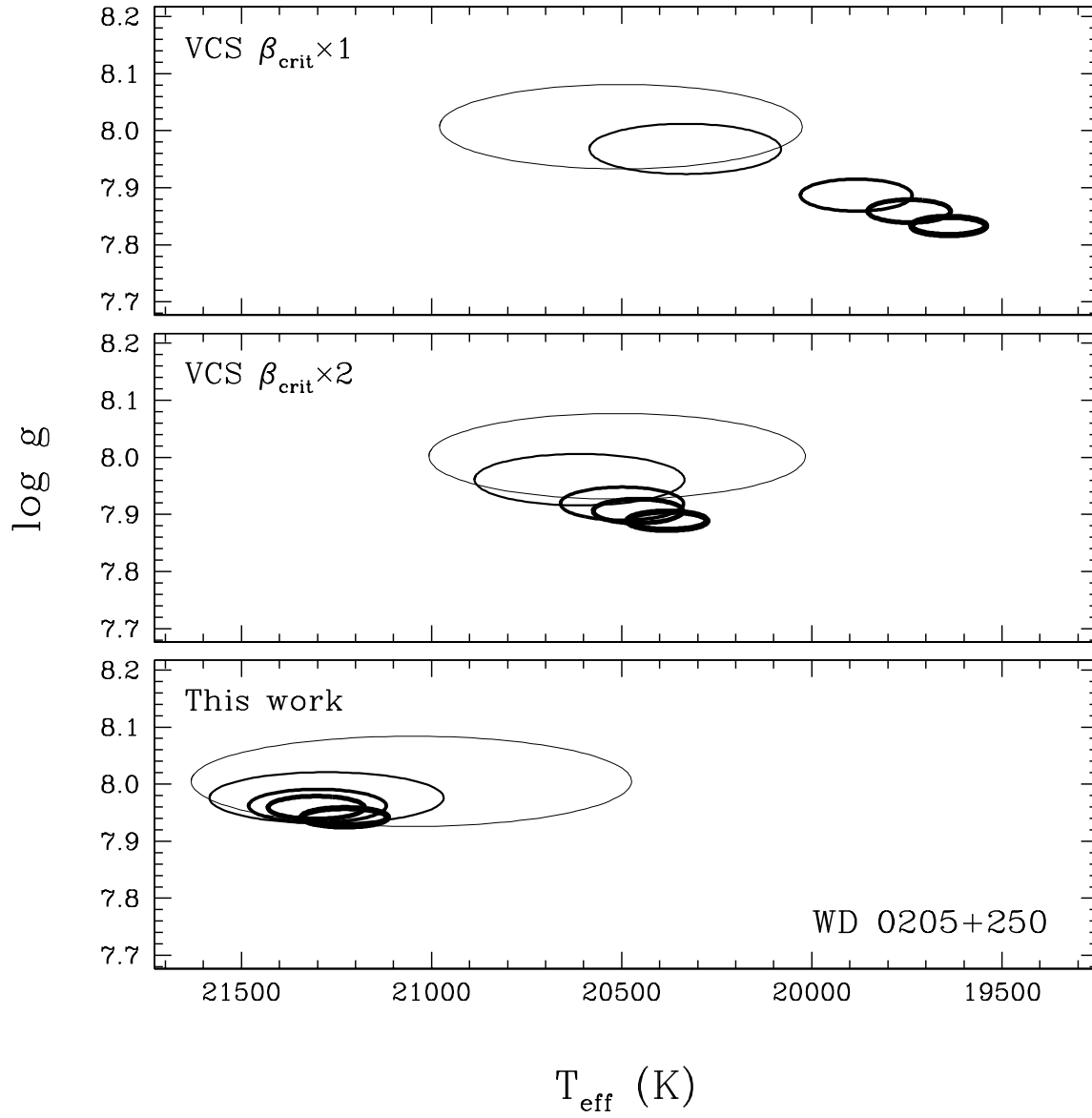


Figure 2

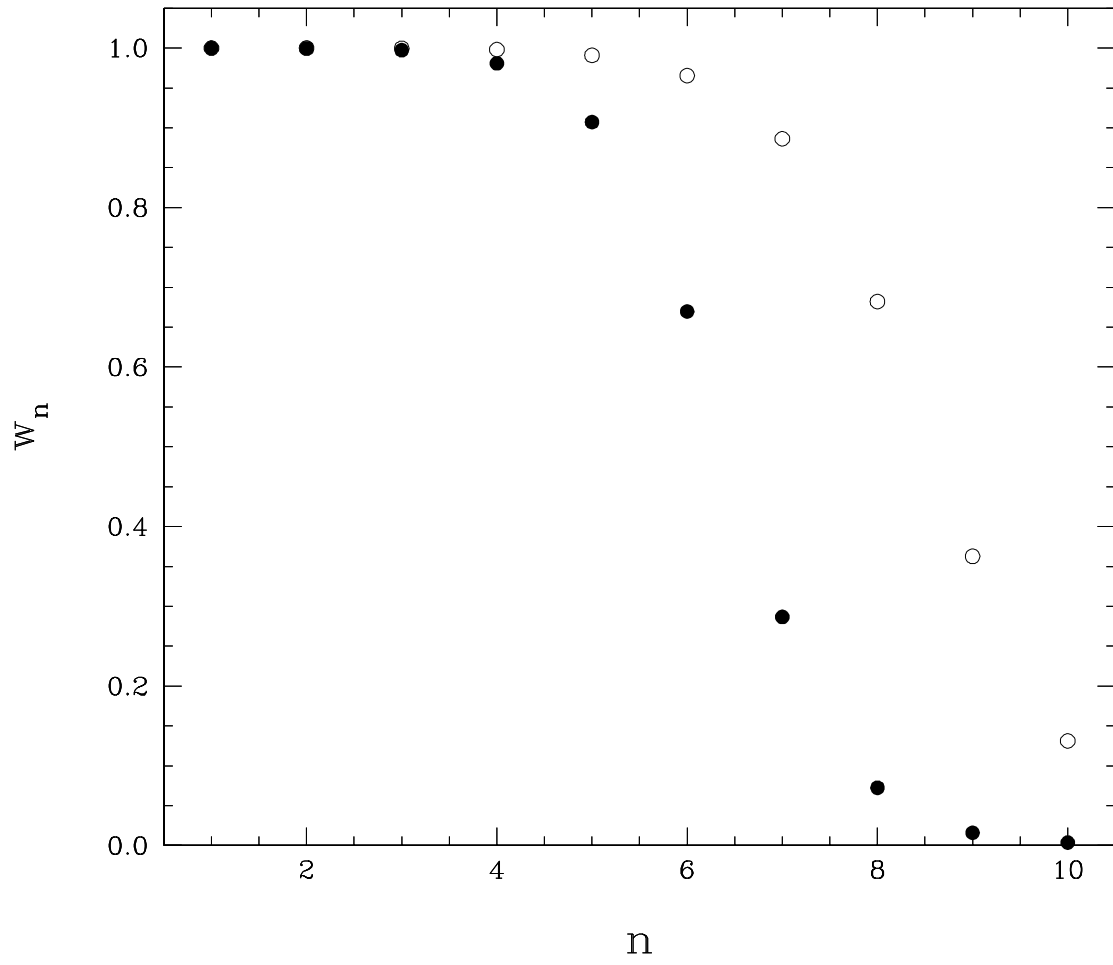


Figure 3

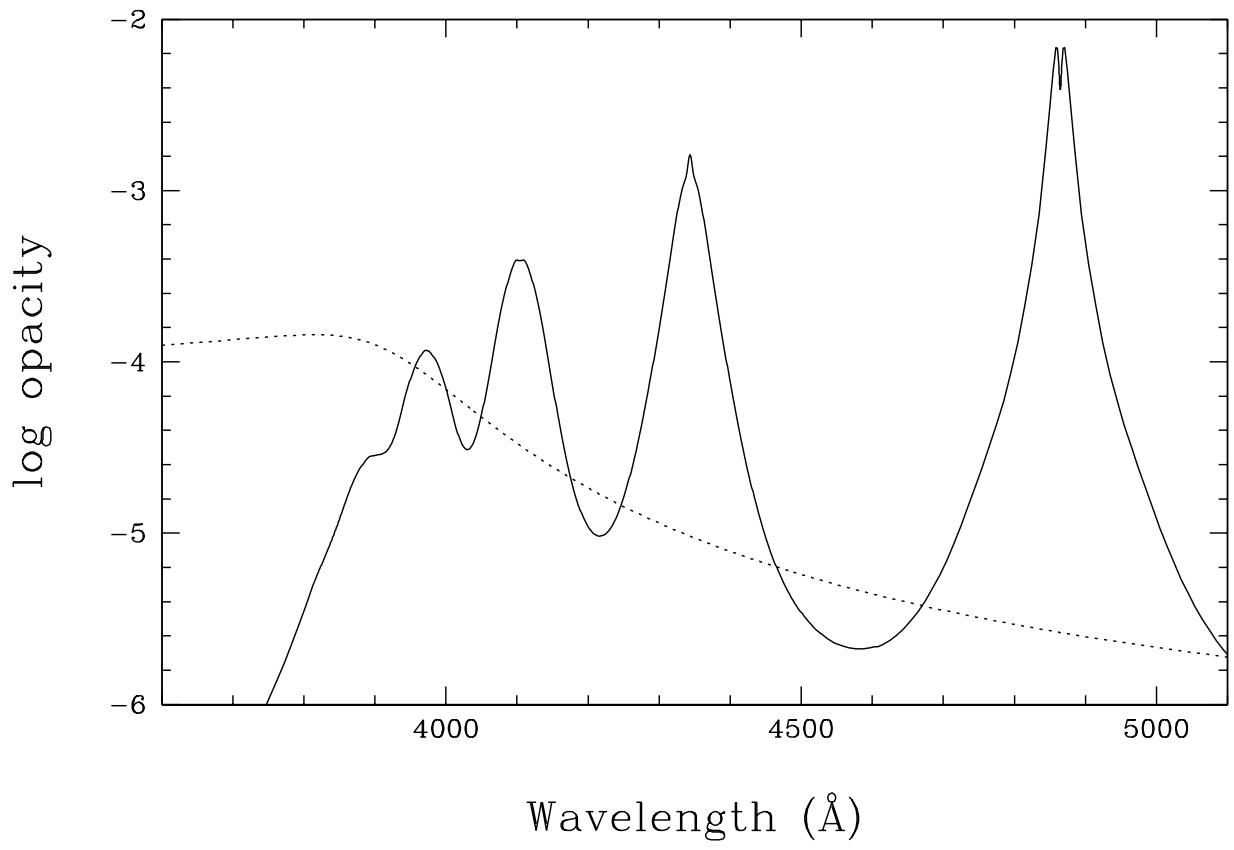


Figure 4

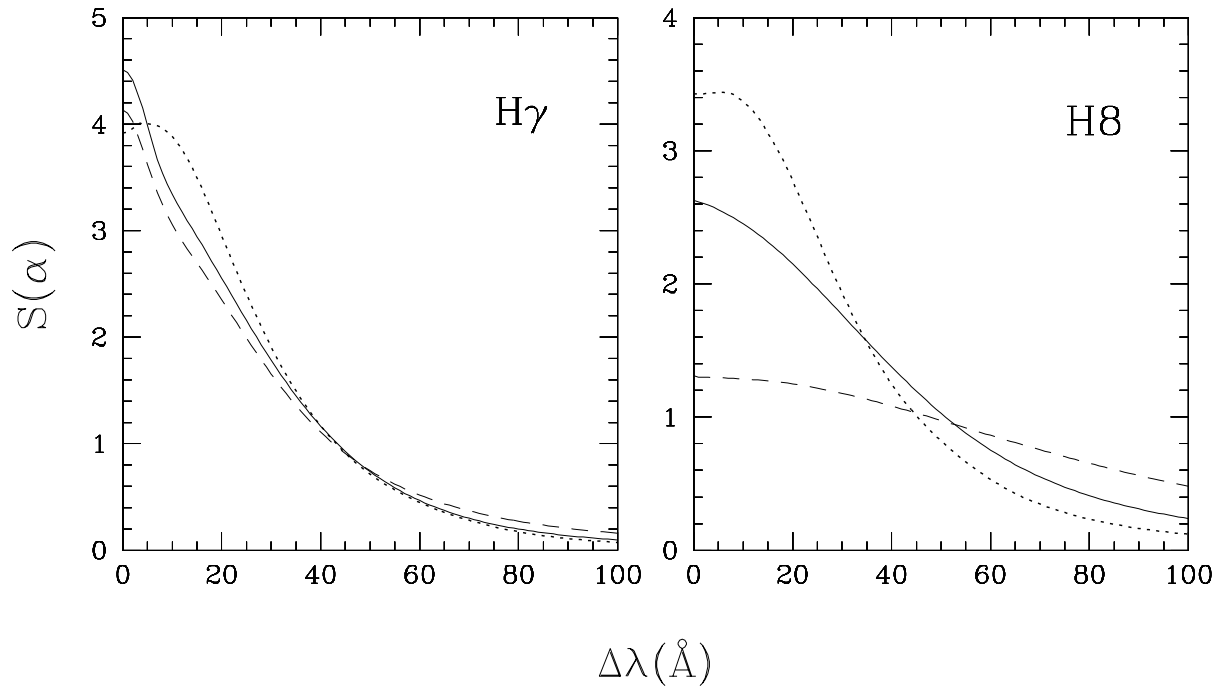


Figure 5

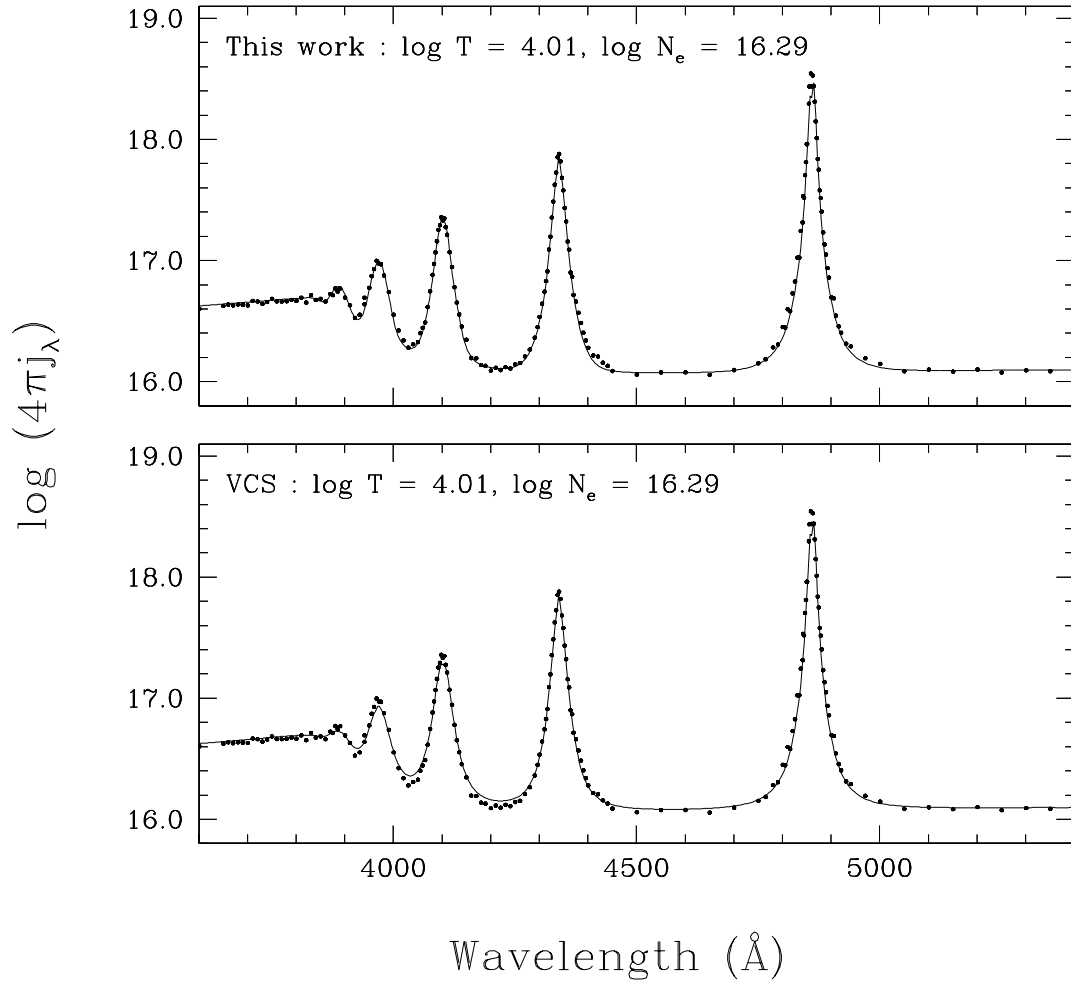


Figure 6

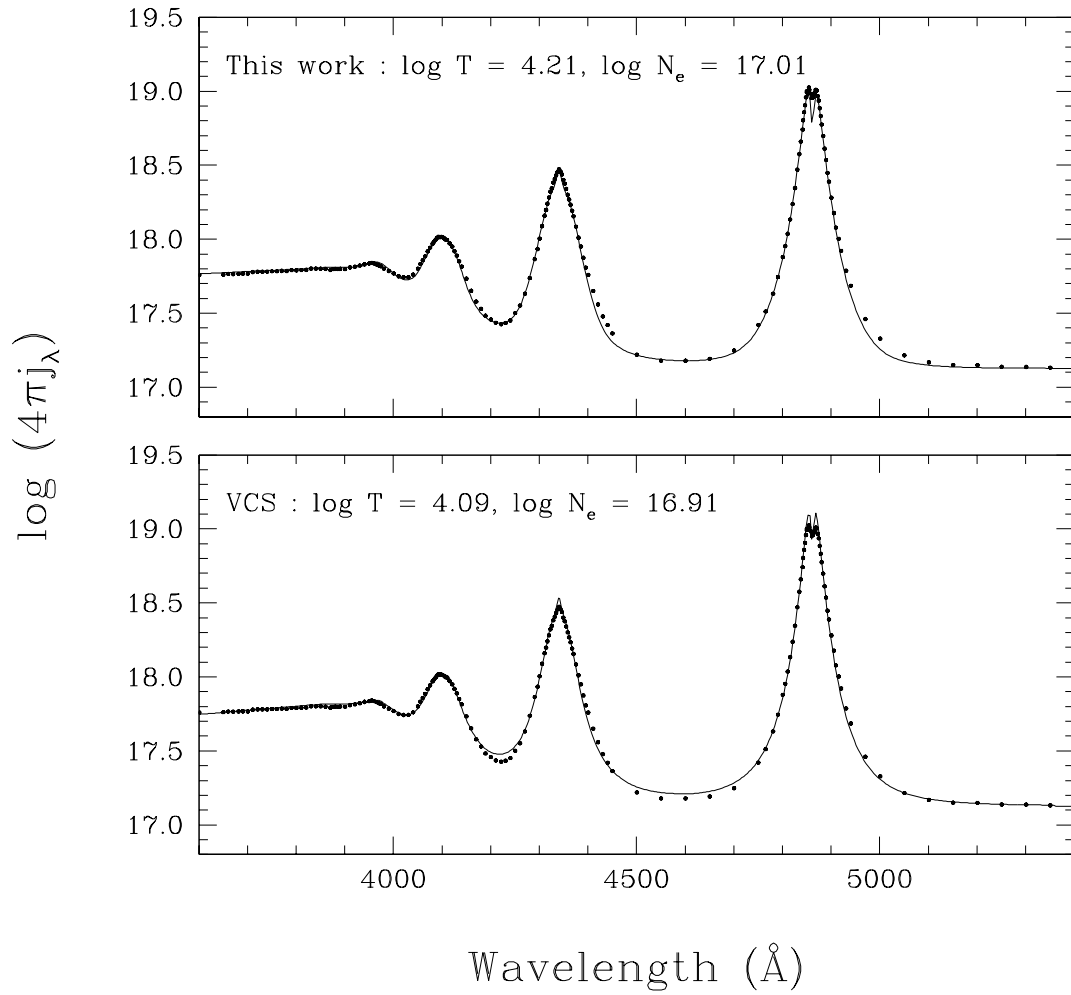


Figure 7

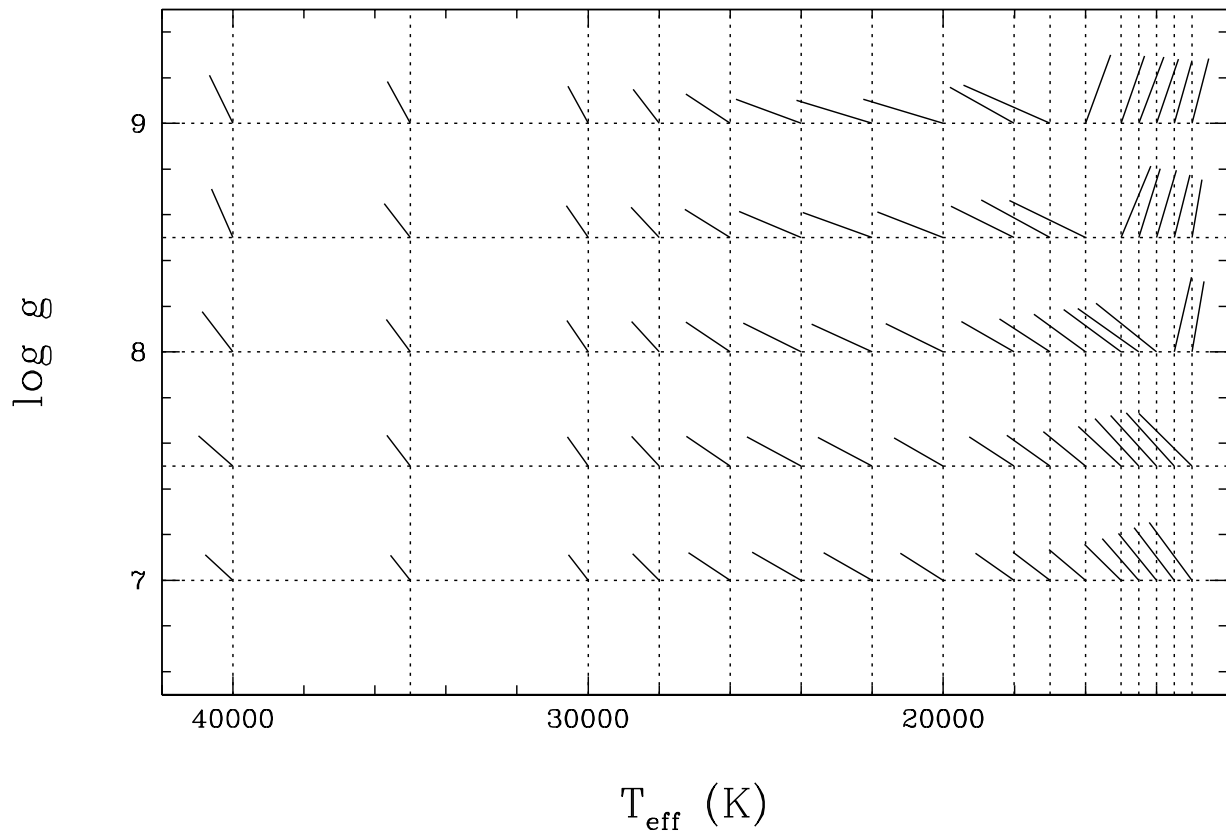


Figure 8

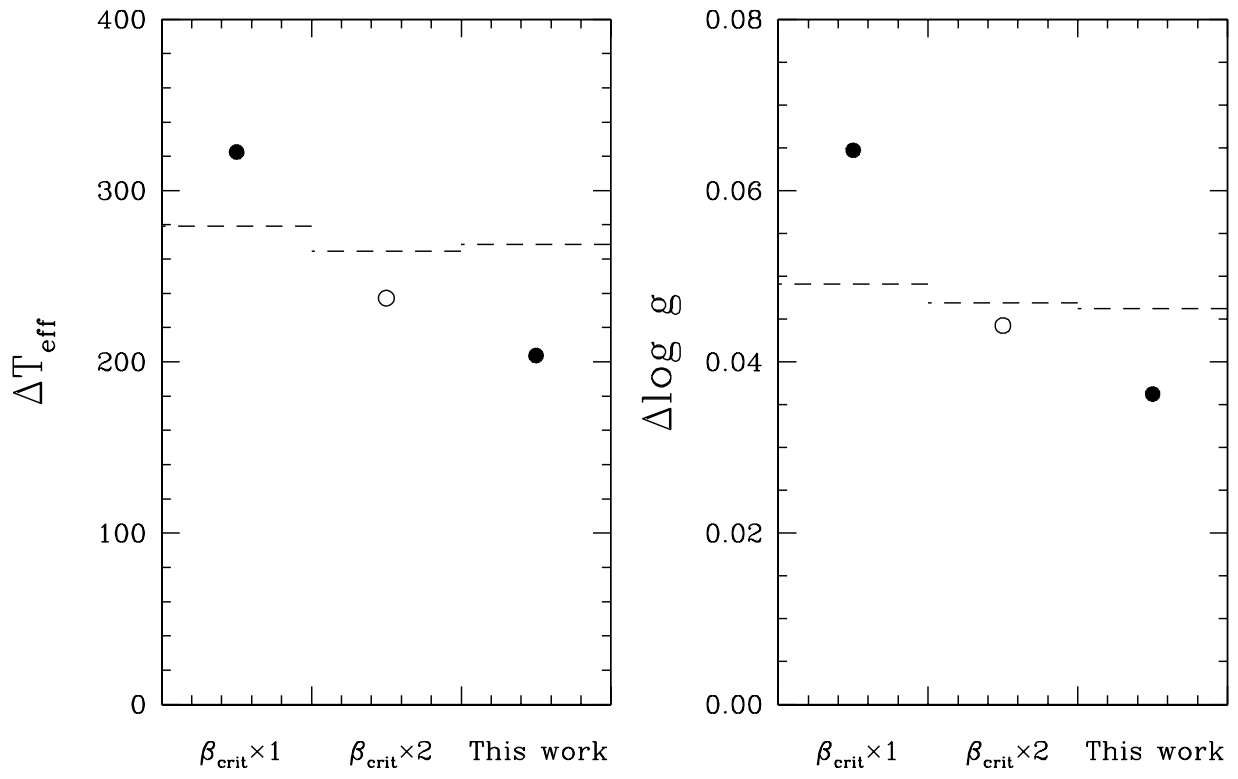


Figure 9

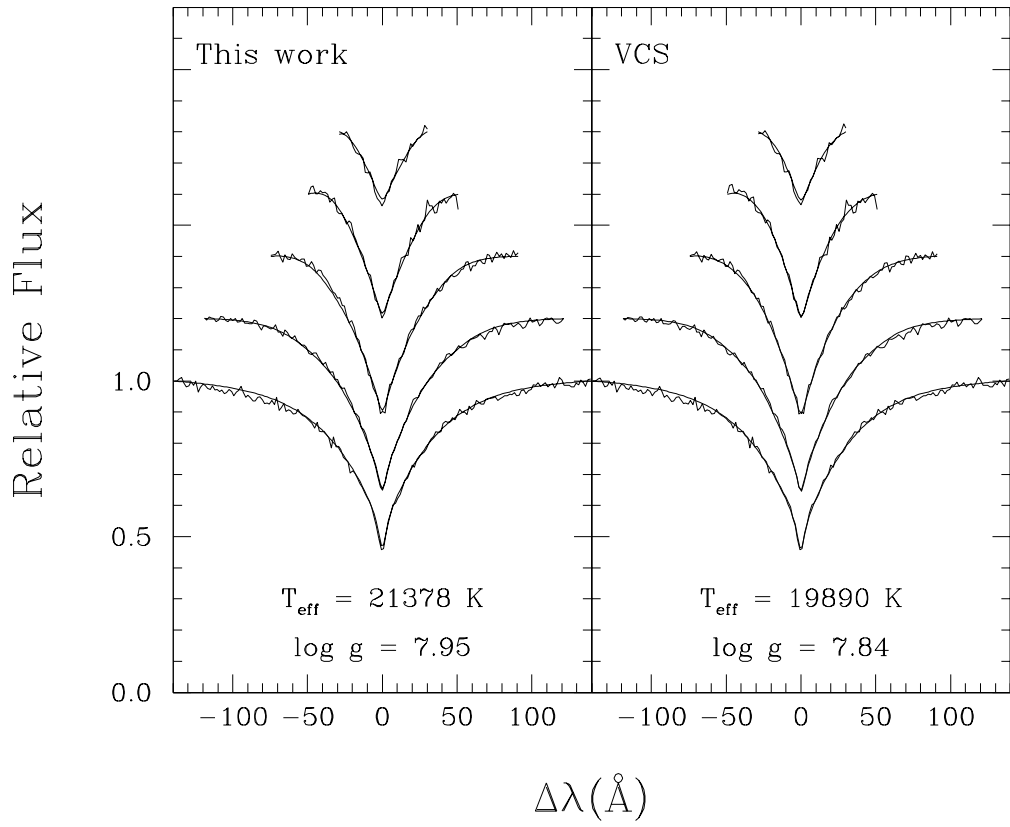


Figure 10

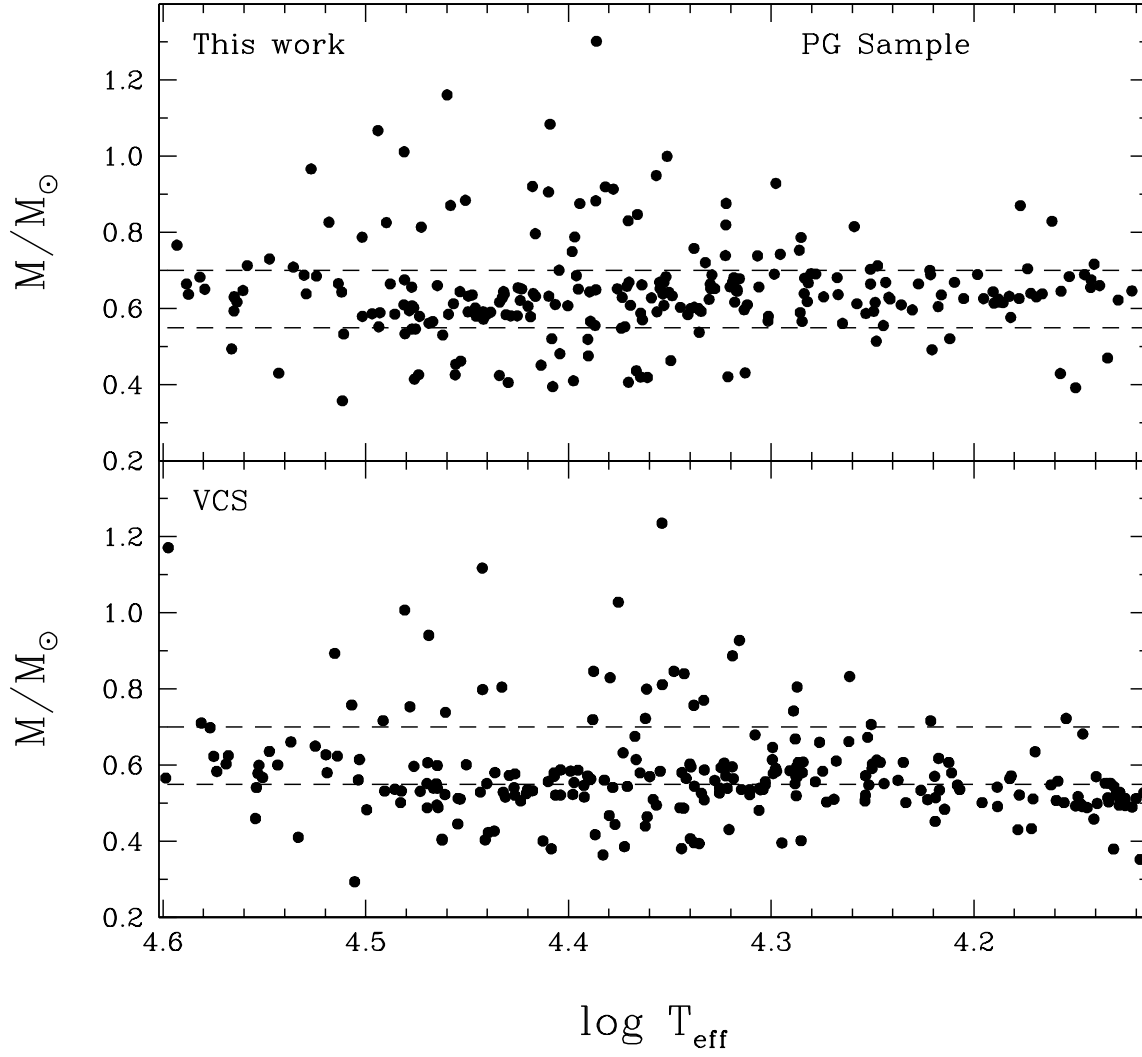


Figure 11

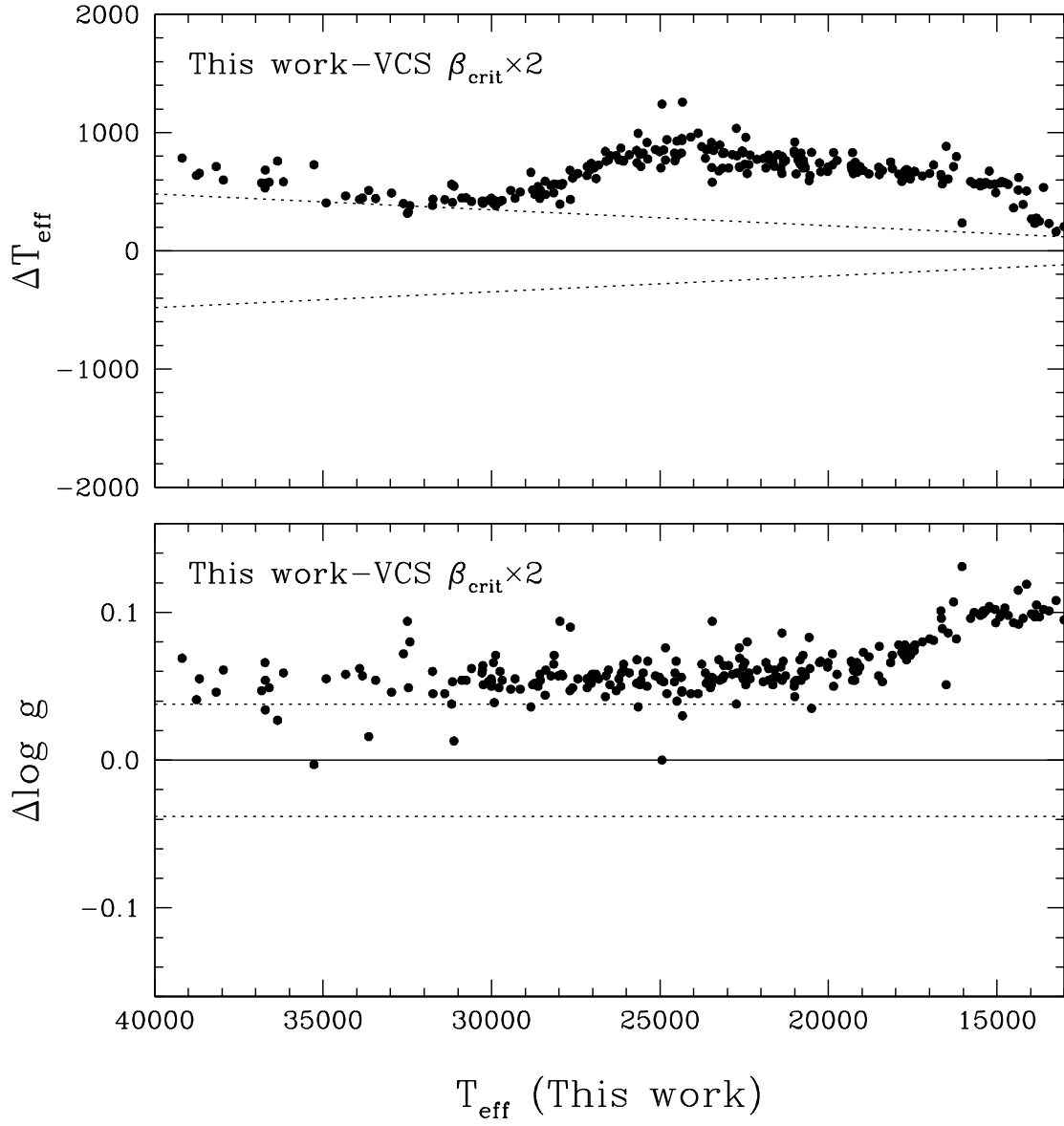


Figure 12

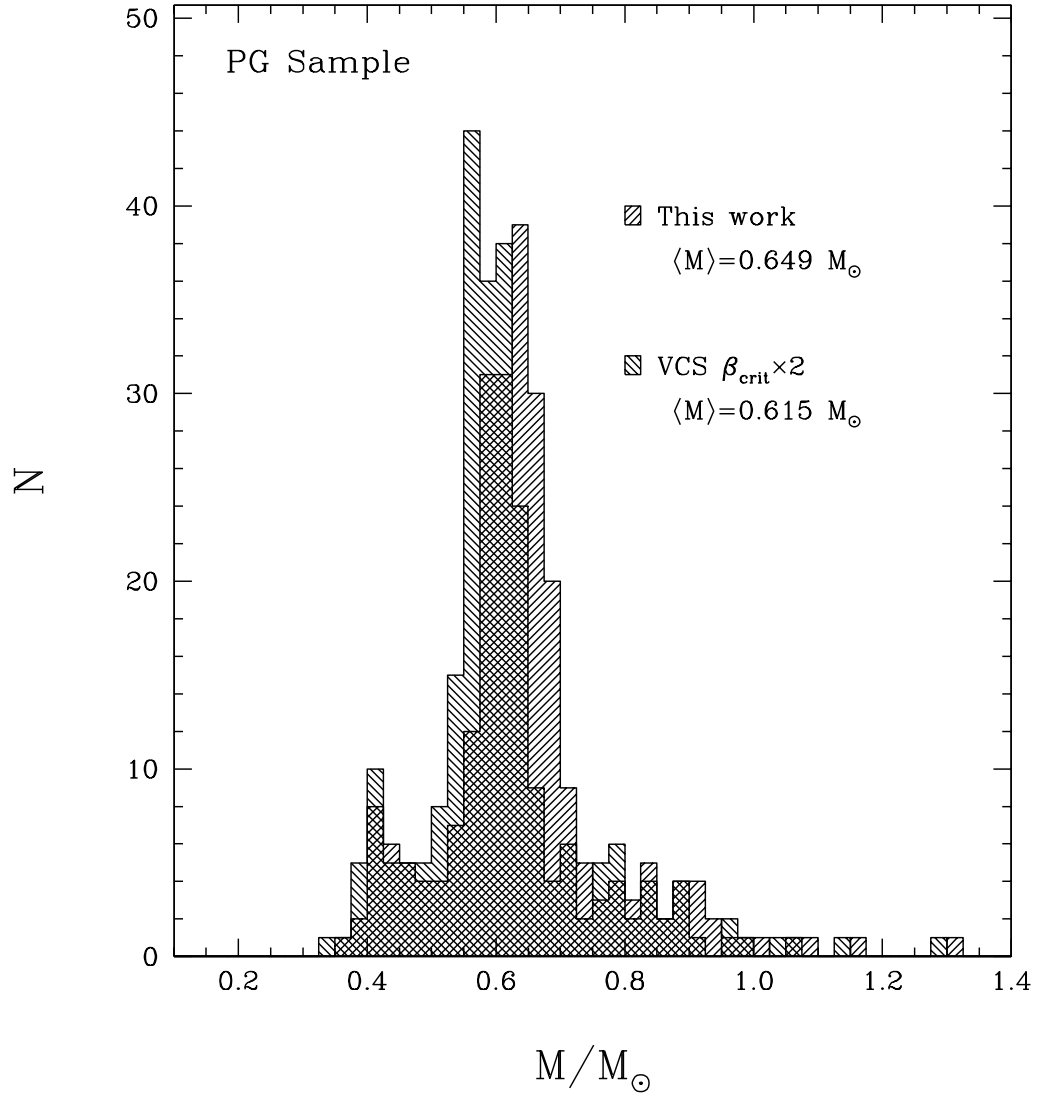


Figure 13

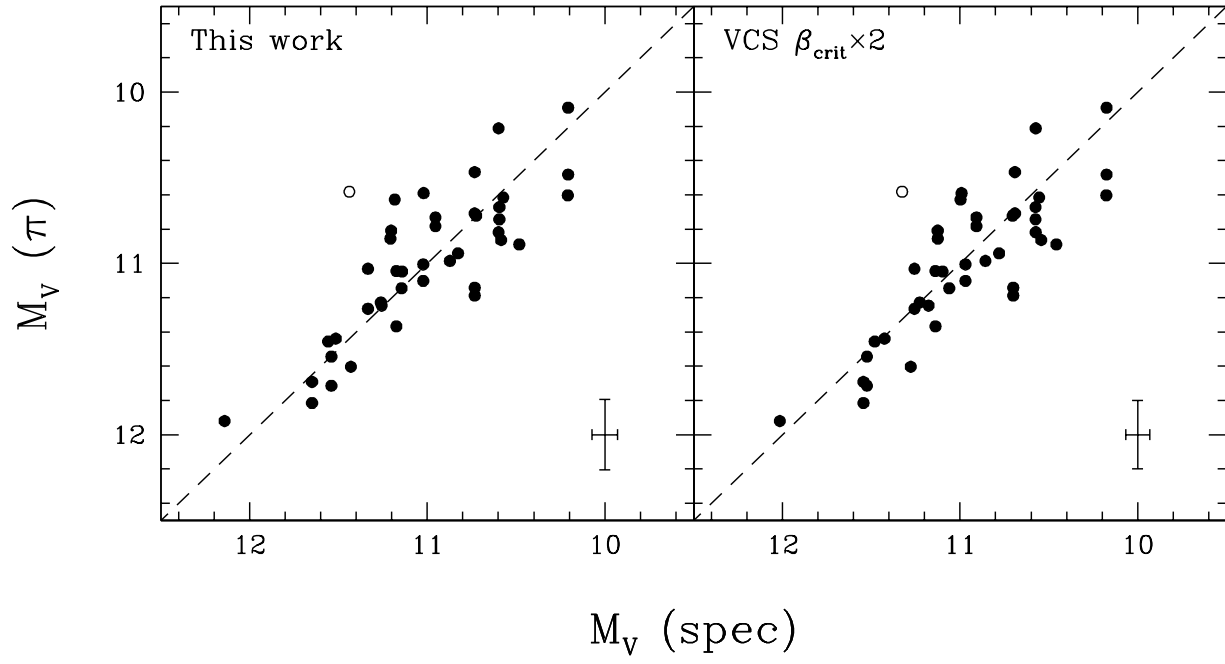


Figure 14